**Distribution Agreement**

In presenting this thesis as a partial fulfillment of the requirements for a degree from Emory University, I hereby grant to Emory University and its agents the non-exclusive license to archive, make accessible, and display my thesis in whole or in part in all forms of media, now or hereafter now, including display on the World Wide Web. I understand that I may select some access restrictions as part of the online submission of this thesis. I retain all ownership rights to the copyright of the thesis. I also retain the right to use in future works (such as articles or books) all or part of this thesis.

Nathaniel Lechtzin April 3, 2023

Influence of epigallocatechin gallate on protein dynamics in oligomeric alpha-synuclein

by

Nathaniel Lechtzin

Kurt Warncke, Ph.D.
Adviser

Physics

Kurt Warncke, Ph.D.

Adviser

Laura Finzi, Ph.D.

Committee Member

Effrosyni Seitaridou, Ph.D.

Committee Member

2023

# Influence of epigallocatechin gallate on protein dynamics in oligomeric alpha-synuclein

By

Nathaniel Lechtzin

Kurt Warncke, Ph.D.

Adviser

An abstract of
a thesis submitted to the Faculty of Emory College of Arts and Sciences
of Emory University in partial fulfillment
of the requirements of the degree of
Bachelor of Science with Honors

Physics

2023

Abstract

Influence of epigallocatechin gallate on protein dynamics in oligomeric alpha-synuclein
By Nathaniel Lechtzin

The intrinsically disordered protein, $\alpha$-synuclein ($\alpha$-syn) plays a role in neurotransmitter release in brain neurons, and its dysfunction is associated with debilitating neurodegenerative disorders, such as Parkinson's disease. Oligomeric forms of $\alpha$-syn have been identified as cytotoxic, owing to proposed membrane disruption and permeabilization. The small molecule, epigallocatechin gallate (EGCG), a polyphenolic compound derived from green tea, has been shown to bind to oligomeric $\alpha$-syn, remodel oligomer structure, inhibit membrane permeabilization, and suppress the dynamics of intrinsically disordered regions within $\alpha$-syn. Here, we employ temperature-controlled ice boundary confinement and spin probe (TEMPOL) electron paramagnetic resonance spectroscopy in frozen solution samples of $\alpha$-syn in the presence of varying concentrations of EGCG (molar ratios of 1, 7, 15, 60 and 100, relative to $\alpha$-syn) to elucidate the mechanism of action of EGCG. The presence of oligomeric $\alpha$-syn was confirmed in our samples by transmission electron microscopy. Simulation of the electron paramagnetic resonance spectra obtained over the temperature range of 225-265 K reveals two distinct motional components, identified by relatively long (slow rotation) and short (fast rotation) TEMPOL rotational correlation times, and corresponding normalized weights. In the presence of EGCG, the fast component retains the mesophase mobility of $\alpha$-syn alone, independent of EGCG concentration over the full temperature range. In contrast, the slow component mobility decreases for EGCG/$\alpha$-syn ratios greater than 1:1, at each temperature value. The fast component dominance (weight≈0.8) at high temperatures transitions to slow component dominance at low temperatures (>0.9). The crossover temperature of equal weights is shifted to higher temperatures by increasing EGCG concentration. The characteristic thermal hysteresis, which arises from compaction of the dynamics of the disordered C-terminal domain of $\alpha$-syn oligomers is also observed in the presence of EGCG. At high concentrations of EGCG (100:1, 60:1) and elevated temperatures, a redox reaction leads to TEMPOL radical annihilation. Together, the results indicate that EGCG associates predominantly with the N-terminal and central, non-amyloid component of the β-sheet-structured oligomer core, rather than the dynamically disordered C-terminal domain, that protrudes from the core. Overall, we find that EGCG attenuates the dynamics of $\alpha$-syn oligomers globally, making $\alpha$-syn more susceptible to confinement.

# Influence of epigallocatechin gallate on protein dynamics in oligomeric alpha-synuclein

By

Nathaniel Lechtzin

Kurt Warncke, Ph.D.

Adviser

A thesis submitted to the Faculty of Emory College of Arts and Sciences
of Emory University in partial fulfillment
of the requirements of the degree of
Bachelor of Science with Honors

Physics

2023

Acknowledgements

I would like to acknowledge my advisor, Dr. Kurt Warncke, for his guidance, knowledge, and flexibility. I would also like to thank the graduate students, Katie Whitcomb and Wei Li, for sharing their combined wisdom. Finally, thank you to the members of my committee, Dr. Finzi and Dr. Seitaridou, for their time and continued support.

## Table of Contents

## List of Figures

## Introduction

### 1. The α-synuclein protein

The monomeric protein, $\alpha$-synuclein ($\alpha$-syn), is an intrinsically disordered protein (IDP) under physiological conditions *in vitro.*[1] $\alpha$-Syn is localized within the presynaptic nerve axon terminal (i.e., synaptic bouton), and it plays a hitherto unspecified role in neurotransmitter release.[2] Dysfunction of $\alpha$-syn is associated with Parkinson's Disease (PD), the second most common neurodegenerative disease in humans, and several other neurodegenerative disorders known as synucleinopathies.[3] $\alpha$-Syn is comprised of 140 residues (14.5 kDa) and human $\alpha$-syn is encoded by the SNCA gene. $\alpha$-Syn is composed of three distinct regions. The N-terminal domain (NTD; residues 1-60) consists of repeated 11-residue domains and has a propensity to form an amphipathic $\alpha$-helix, promoting interactions with phospholipid membranes.[2,4] The central region (residues 61-95) is hydrophobic, prone to aggregation, and constitutes the non-amyloid-$\beta$ component (NAC) of $\alpha$-syn.[5] In the presence of lipid vesicles and phospholipid membranes, the NTD and NAC take on an $\alpha$-helical structure, allowing $\alpha$-syn to bind to the membrane surface.[6] Upon association, $\alpha$-syn can alter the organization and stability of membranes, and this membrane binding and remodeling is implicated in the physiological role of $\alpha$-syn as a modulator of neurotransmitter release.[7,8] Furthermore, $\alpha$-syn has been reported to exhibit chaperone activity, assisting in the repeated assembly and disassembly of the soluble N-ethyl-maleimide-sensitive factor (NSF) attachment protein receptor (SNARE) complex, a process that is necessary for the repeated release of neurotransmitters.[9] $\alpha$-Syn is also associated with the facilitation and attenuation of synaptic vesicle pooling and recycling.[10]

The C-terminal domain (CTD; residues 96-140) contains a preponderance of acidic residues and prolines and is implicated in interactions between $\alpha$-syn and other proteins, such as VAMP2 (vesicle associated membrane protein 2).[11] The CTD is an intrinsically disordered region (IDR), and it remains free and unfolded during membrane binding.[12] Monomeric $\alpha$-syn has the capacity to aggregate,[13,14] which leads to the formation of several types of partially ordered structures, including multimers, liquid-liquid phase separation,[15–18] oligomers,[19] and fibrils, for all of which the CTD remains dynamic and free.[20–23]s

## 2. Aggregate forms of α-synuclein

Neurodegenerative conditions associated with $\alpha$-syn are hallmarked by the accumulation of excess $\alpha$-syn, which, in the case of PD and other Lewy Body Diseases (LBD), gives rise to the buildup of Lewy bodies, intracellular protein aggregates of varying morphologies considered the defining feature of LBD pathologies.[3,24] $\alpha$-Syn is the major component of Lewy bodies in PD.[25] $\alpha$-Syn oligomer size can vary from dimers to dozens of monomers, with significant heterogeneity in structure depending on solution conditions and methods of preparation.[26] For example, lyophilization is a common approach for generating $\alpha$-syn samples rich in stable oligomeric species, yet this preparation method produces a highly polydisperse distribution of oligomer sizes.[27] Oligomers most commonly assume an ellipsoid, disc-like ultrastructure, consisting of a core with partial secondary structure rich in $\beta$-sheets (predominantly the NAC and, to a lesser extent, the NTD), surrounded by the dynamic and unstructured CTDs.[28] a-Syn also forms fibrils, whose core structure of $\alpha$-syn fibrils has been resolved by solid-state nuclear magnetic resonance (NMR) spectroscopy,[21] as well as cryogenic electron microscopy (cryo-EM).[22,23] The fibril core is composed primarily of parallel $\beta$-sheets (NAC) with the NTD and

CTD IDRs protruding outward along the length of the fibril. The structure of the IDRs remains poorly characterized owing to their disorder and dynamism. Oligomers of $\alpha$-syn display an intermediate amount of secondary structure content, with a fraction of $\beta$-sheet structure in between those observed in monomers (i.e., no well-defined secondary structure) and $\alpha$-syn fibrils, which contain the greatest amount of $\beta$-sheet structure among the aggregated states of $\alpha$-syn.[27] The transient nature of $\alpha$-syn oligomers, on the NMR time scale of microseconds to milliseconds, as well as the substantial heterogeneity in their size and structure, have hindered efforts to directly quantify them or describe their structure in detail.[26]

**3. Effects of the polyphenolic antioxidant, (-)-Epigallocatechin gallate (EGCG), on peptide aggregate structures**

(-)-Epigallocatechin gallate (EGCG) is a polyphenol and powerful antioxidant derived from green tea (Fig. 1). Consistent with the amphipathic nature of the NTD, EGCG displays a distinct affinity for this region of $\alpha$-syn, and, generally, each $\alpha$-syn monomer may bind up to 54 EGCG molecules during oligomerization, whereas pre-formed $\alpha$-syn oligomers are able to bind up to approximately 7 molecules of EGCG for each $\alpha$-syn.[29] Phenolic compounds have been demonstrated to hinder aggregation of $\alpha$-syn.[30] EGCG has been shown to potently inhibit $\alpha$-syn aggregation into oligomers, and it promotes disaggregation of existing $\alpha$-syn oligomers.[31] Additionally, EGCG reportedly reduces $\alpha$-syn oligomer cytotoxicity by inhibiting the ability of oligomers to associate with and permeabilize membranes, without significant effects on the oligomers' size or secondary structure.[32] Contrary to the effects of non-treated oligomers,[33] oligomers exposed to EGCG are also not reported to reduce mitochondrial activity or induce production of reactive oxygen species (ROS).[30,34] There is also evidence that EGCG redirects the

fibrillation of $\alpha$-syn, configuring aggregating $\alpha$-syn monomers into non-toxic, off-pathway oligomers and restructuring existing fibrils into non-toxic aggregate structures.[35,36] The neuroprotective and therapeutic potential of EGCG makes it a highly desirable target for further study.

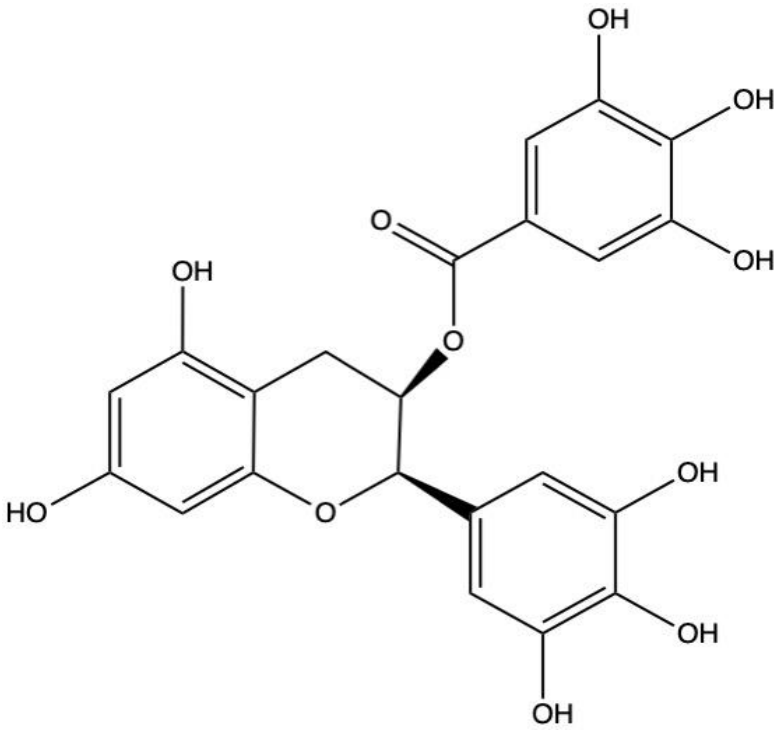


*Figure 1.* Structure of the small molecule, EGCG, with its di-hydroxy and two tri-hydroxy-substituted phenyl rings; small molecules containing aromatic components with multiple vicinal hydroxyl groups have been reported to effectively inhibit aggregation of $\alpha$-syn into oligomers and to disaggregate pre-formed $\alpha$-syn oligomers.[31]

**4. Low-temperature frozen aqueous mesodomain system**

In the present study, *in vivo* intracellular confinement is paralleled by the ice boundary in frozen aqueous solution. Freezing of aqueous solutions leads to the exclusion of impurities, such as proteins or solutes, from the encroaching ice front and thus to localization within interstitial regions of the polycrystalline bulk ice.[37] Protein motions are tightly coupled to dynamics of the surrounding solvent.[38,39] The present system thus consists of protein in the polycrystalline ice-bounded, interstitial, aqueous mesodomain, or freeze-concentrated liquid surrounding the protein.[40] The electron paramagnetic resonance (EPR) spin probe, TEMPOL, a small heterocyclic molecule and stable aminoxyl radical, is also excluded by the ice front and is thus localized to the solvent domains directly surrounding the protein. For folded, globular proteins, TEMPOL is localized in a hydration layer most immediately surrounding the protein surface, or protein-associated domain (PAD), and the solvent mesodomain, the next concentric layer between the protein surface and the ice boundary. The PAD and mesodomain solvent components are identified by rotational correlation time ($\tau_c$; determined from theory-based simulation of EPR line shape),[41] which directly reflects the solvent phase mobility and, by extension, the protein-coupled solvent dynamics.[42,43,44] TEMPOL can reveal the dynamical condition of the PAD and mesodomain solvent phases over a window of detectable correlation times ~$10^{-10} \leq \tau_c \leq 10^{-7}$ s at a microwave frequency of about 9.5 GHz.[45] The previous EPR studies of aqueous globular proteins frozen in the presence of cryosolvents, solvents that remain liquid at low temperatures, have found two distinguishable mobility components that correspond to distinct solvent phases.[46] The slow mobility component is associated with the fraction of TEMPOL within the PAD, and the fast mobility component is considered to correspond to

TEMPOL in the mesodomain, which envelops the PAD and is externally enclosed by polycrystalline ice.[42] Cryosolvents are generally precluded from the PAD and thus contribute only to the volume of the mesodomain.[42,47] Therefore, no mesodomain layer is observed in the absence of added cryosolvent such that the PAD is directly bordered by the polycrystalline ice boundary.[48]

**5. Spin-probe electron paramagnetic resonance (EPR) spectroscopy**

The TEMPOL spin probe is randomly oriented in the EPR samples, with respect to the external magnetic field. The EPR spectra of TEMPOL arise from the interactions of the unpaired electron spin ($S$=1/2) with the external magnetic field (Zeeman interaction; defined by the $\boldsymbol{g}$ tensor) and the nitroxide $^{14}$N nuclear spin ($I$=1) through the hyperfine interaction (defined by the $^{14}$N hyperfine tensor). The energy level diagram is shown in Fig. 2. The $^{14}$N hyperfine interaction is dominant at the X-band microwave frequencies and magnetic fields used in the reported experiments. The spectral features correspond to electron spin-spin transitions ($\Delta m_s=\pm 1/2$), and the three-line spectrum arises from the electron spin transitions among the three $^{14}$N nuclear spin states, defined by $m_I$=0, ±1.[49] Figure 3 shows that effect of rotational motion of the TEMPOL spin probe on the EPR line shape. At higher temperatures, the relatively rapid rotational motion of the spin probe averages the dipolar hyperfine interaction, which leads to the clear resolution of three spectral features, which are separated by the isotropic (through-bond coupling; not orientation-dependent) $^{14}$N hyperfine coupling constant. Slower rotation at lower temperatures leads to manifestation of the orientation-dependent dipolar hyperfine interaction, which broadens each $m_I$ feature. In the rigid limit, corresponding to a rotational correlation time ($\tau_c$) of $>10^{-7}$ s, the full, anisotropically broadened, or "powder-pattern" line shape is manifested.

These effects of motion on the TEMPOL line shape are the basis for extraction of $\tau_c$ and component weights, *W*, by using EPR simulations.[41,45]

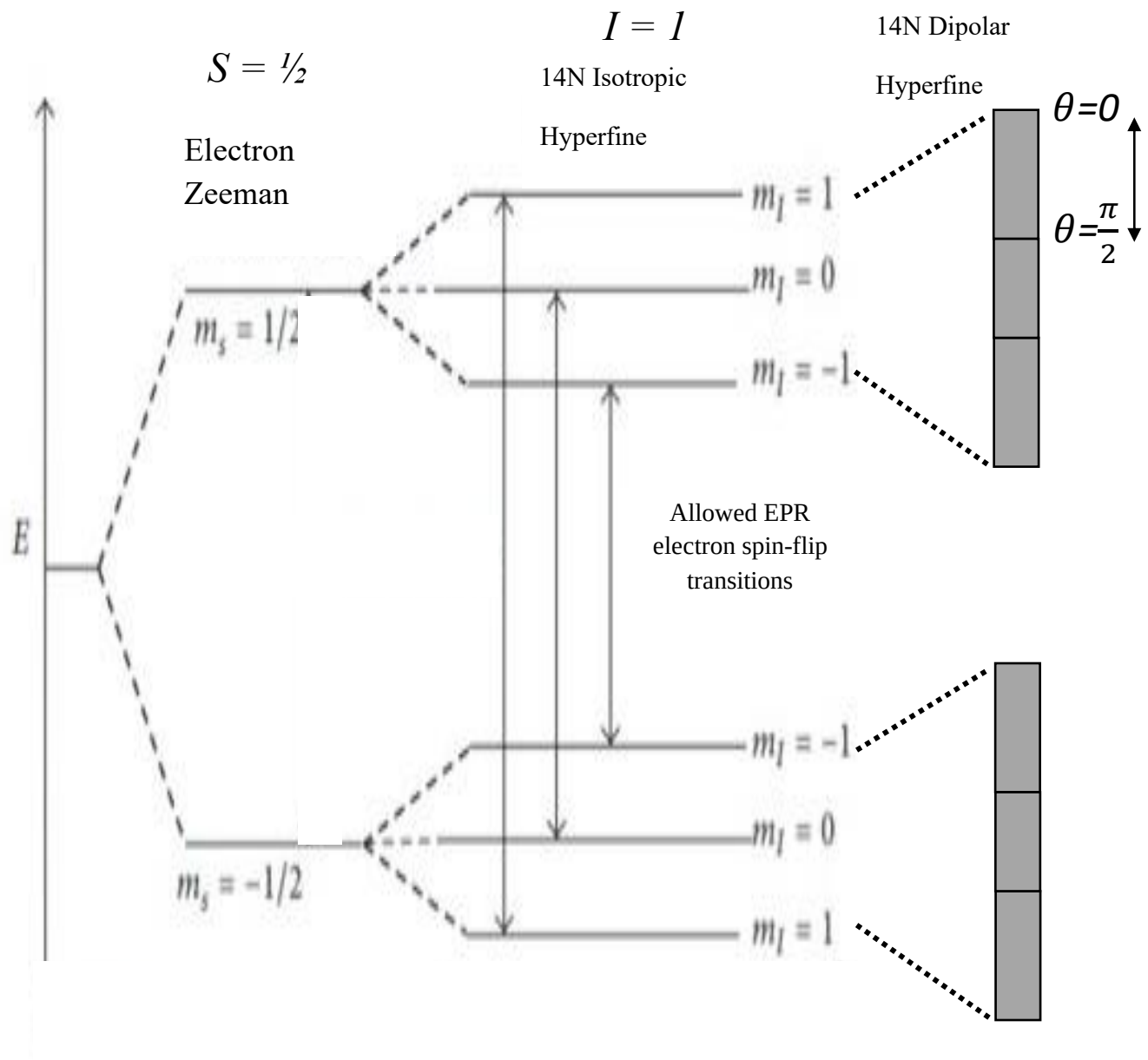


*Figure 2.* Energy level diagram for the nitroxide spin probe, TEMPOL. Succession of states, from left to right: (1) In the absence of a magnetic field, the two spin states of the unpaired electron ($S$=1/2) on TEMPOL, $m_s$=±1/2, are degenerate in energy. (2) In the presence of an external magnetic field, the degeneracy is lifted, and the energy difference between "spin up" and "spin down" states is equal to the electron Zeeman splitting, $\Delta E = g_e \beta B_0$, where $g_e$ is the electron g-factor, β is the Bohr magneton, and $B_0$ is the external magnetic field magnitude. (3) In TEMPOL, the unpaired electron spin is coupled to the $^{14}$N nucleus ($I$=1, $m_I$=0, ±1) of the

nitroxide moiety. The nuclear Zeeman effect leads to the same energy shifts in each electron spin manifold, and so does not influence observed transition energies. The electron-nuclear, or hyperfine, interaction between electron and $^{14}N$ leads to the hyperfine splitting. When the microwave energy ($E=h\nu$; $h$, Planck's constant; $\nu$, microwave frequency, ~9.5 GHz) matches the energy level splitting for the electron spin states, electron spin-flip transitions occur, in accord with the indicated selection rules, with net absorption of energy. At higher temperatures, the relatively mobile spin probe rotationally averages the electron-nuclear dipolar part of the hyperfine coupling, and three distinct lines are observed, that are separated by the isotropic (through-bond) hyperfine coupling. As the temperature is lowered, progressive probe immobilization leads to the manifestation of the dipolar coupling, and the spectrum broadens, reaching the rigid-limit line shape when the rotational correlation time is $>10^{-7}$ s.

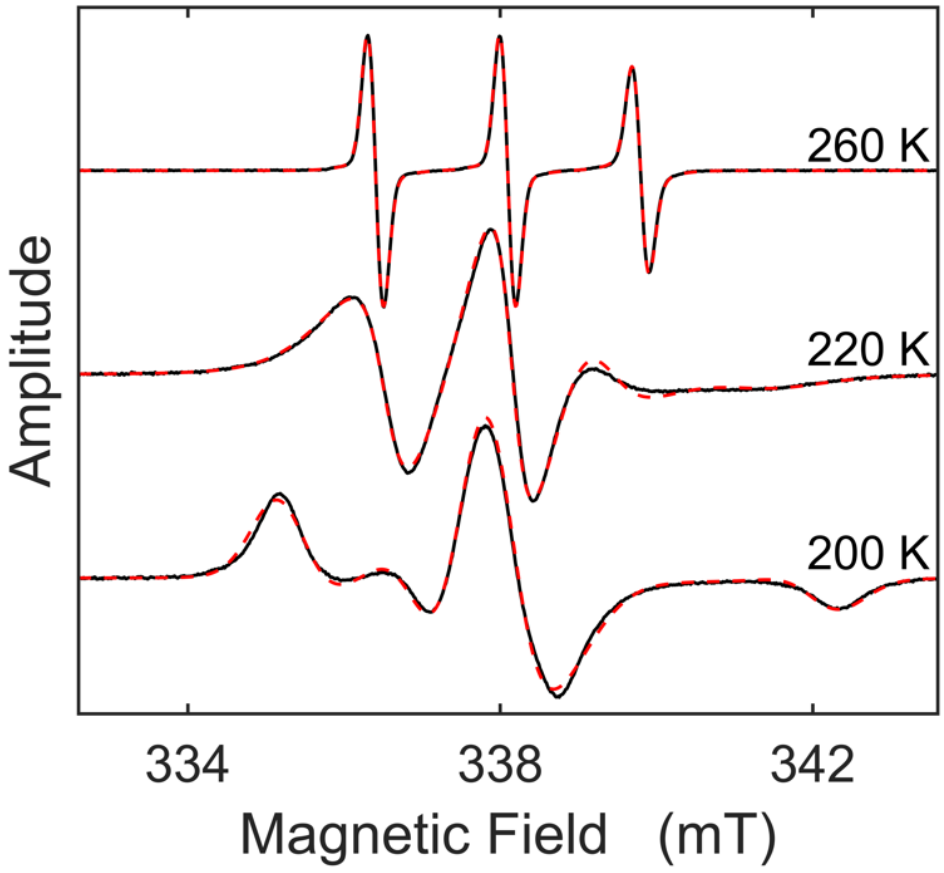


*Figure 3.* Representative single-component TEMPOL EPR spectra in the frozen aqueous solution mesodomain system, showing three general regimes of TEMPOL mobility. Experimental spectra (black) display the characteristic rigid limit (200 K), intermediate rotational mobility (220 K) and rapid tumbling (260 K) line shapes. EPR simulations are shown overlaid (red dashed lines). The correlation times are as follows: 200 K: $\tau_c=4.57\times10^{-8}$ s; $\log\tau_c=-7.34$; 220 K: $\tau_c=3.31\times10^{-9}$ s; $\log\tau_c=-8.48$; 260 K: $\tau_c=1.38\times10^{-10}$ s; $\log\tau_c=-9.86$. The samples included TEMPOL (0.2 mM) in the frozen solution mesodomain system prepared by using 2% v/v dimethyl sulfoxide, in the absence of protein. Adapted from (Li et al., 2022, *PCCP*).

## 6. Prologue

Given the incomplete understanding of the physiological function of $\alpha$-syn, in conjunction with the significant human cost of its associated pathologies, it is salient to further clarify the dynamics of $\alpha$-syn as well as potential avenues for generating therapies for synucleinopathies. Here, we employ temperature-controlled, ice boundary confinement to emulate vesicular and protein confinement conditions *in vivo*, and spin probe electron paramagnetic resonance (EPR) spectroscopy,[42,43,48] to interrogate the dynamics of $\alpha$-syn oligomers in the presence of EGCG. The goal is to characterize the molecular mechanistic features of the $\alpha$-syn-EGCG interaction, toward rationalizing the reported therapeutic properties of EGCG and polyphenolic compound, in general.[31,32] The properties of the $\alpha$-syn-EGCG interaction also provide a stringent test of the model for the confinement-resistant dynamics of $\alpha$-syn, as previously described.[50] The EGCG is varied over the wide EGCG: $\alpha$-syn molar ratio range of 1:1 to 100:1. We find that EGCG exerts a selective, concentration-dependent effect on the slow component of the $\alpha$-syn dynamics, while the fast component dynamics are not influenced. Overall, EGCG enhances the confinement of the $\alpha$-syn oligomers, without significant effect on the mobility of the dynamically disordered CTD.

## Materials and methods

### Preparation of EPR samples

All chemicals were from commercial sources. Oligomeric human α-syn was obtained from lyophilized powder (rPeptide, Athens, Georgia, US; P/N S-1001-2). The lyophilized powder was suspended to 1 mg/ml in water (deionized, resistivity 18.2 MW cm), with brief vortex mixing (10-15 s). EPR samples contained 0.5 mg/ml of α-syn in 10 mM potassium phosphate buffer (pH 7.4), with TEMPOL added from freshly prepared stock solution to 0.02 mM. The total sample volume was 0.3 mL. For samples containing EGCG, EGCG was obtained from amorphous solid powder (Sigma-Aldrich, St. Louis, MO). The powdered EGCG was dissolved in water to a concentration of 4 mg/mL. This EGCG stock solution was further diluted for low-[EGCG] samples. EPR samples contained 0.5 mg/mL ([$\alpha$-syn] = 34.5 mM), 34.5 mM, 241.5 mM, 517.5 mM, 2.07 M, and 3.45 M EGCG, respectively (corresponding to molar ratios of 100:1, 60:1, 15:1, 7:1, and 1:1), 0.02 mM TEMPOL, and 10 mM potassium phosphate buffer (pH 7.4), for a total sample volume of 0.3 mL. Samples were transferred to EPR tubes (4 mm outer diameter; Wilmad-LabGlass, Buena, NJ, US), and then frozen by immersion in isopentane at 140 K. EPR samples were stored in liquid nitrogen, prior to measurements.[40]

### Continuous-wave (CW) EPR spectroscopy

X-band CW-EPR spectroscopy was performed on a Bruker E500 ElexSys EPR spectrometer and ER 4123SHQE X-band cavity resonator, with temperature calibration and control.[51] The following acquisition parameters were used: microwave frequency, 9.5 GHz; microwave power, 0.2 mW; magnetic field modulation, 0.2 mT; modulation frequency, 100 kHz. Four to eight spectra were averaged at each temperature.

**Transmission electron microscopy**

Following EPR measurements, frozen $\alpha$-syn and $\alpha$-syn+EGCG samples were thawed and used for TEM sample preparation. EM grids (thick carbon, 400 mesh, copper grids; Electron Microscopy Sciences, Hatfield, PA, US) were cleaned by glow discharge. A grid was placed on top of a 60 µL droplet of each EPR sample for 5 min. The grid was then transferred to the top of a droplet of 2% uranyl acetate for 1 min. Grids were thoroughly dried before imaging, and images were obtained using a JEOL JEM-1400 instrument operating at 80 kV.

**EPR simulations**

Protocols for the simulation of nitroxide EPR spectra in the low-*T* frozen solution system, using the program, EasySpin,[41] and a common set of $\boldsymbol{g}$ and $^{14}$N hyperfine tensor principle values, have been previously described in detail.[40] The correlation times obtained from the simulations are in excellent agreement with those calculated for known solvent viscosity by using the Debye-Stokes-Einstein expression ($\leq$ 2% error for 200 K $\leq T \leq$ 260 K).[48] The rotational correlation times lie within the slow ($\tau_c \rightarrow 10^{-7}$ s) and rapid ($\tau_c \rightarrow 10^{-11}$ s) regimes, that define the bandwidth for CW-EPR detection of rotational motion at X-band.[45]

## Results

### 1. Temperature dependence of TEMPOL EPR line shape in frozen EGCG solution samples

Figure 4 shows EPR spectra over the full range of 200-265 K of temperatures explored for aqueous frozen samples of EGCG. The *T*-varied spectra for EGCG show little dependence on temperature, with the spectra maintaining the TEMPOL EPR rigid-limit line shape throughout the temperature range. The spectra were collected first in order of increasing temperature, with subsequent spectra obtained in the order of decreasing temperature. This rigid-limit line shape is consistent for both increasing- and decreasing-*T* measurements (Fig. 4). There is a minute decrease in derivative amplitude for the decreasing-*T* measurements, but this decrease is constant over the temperature range.

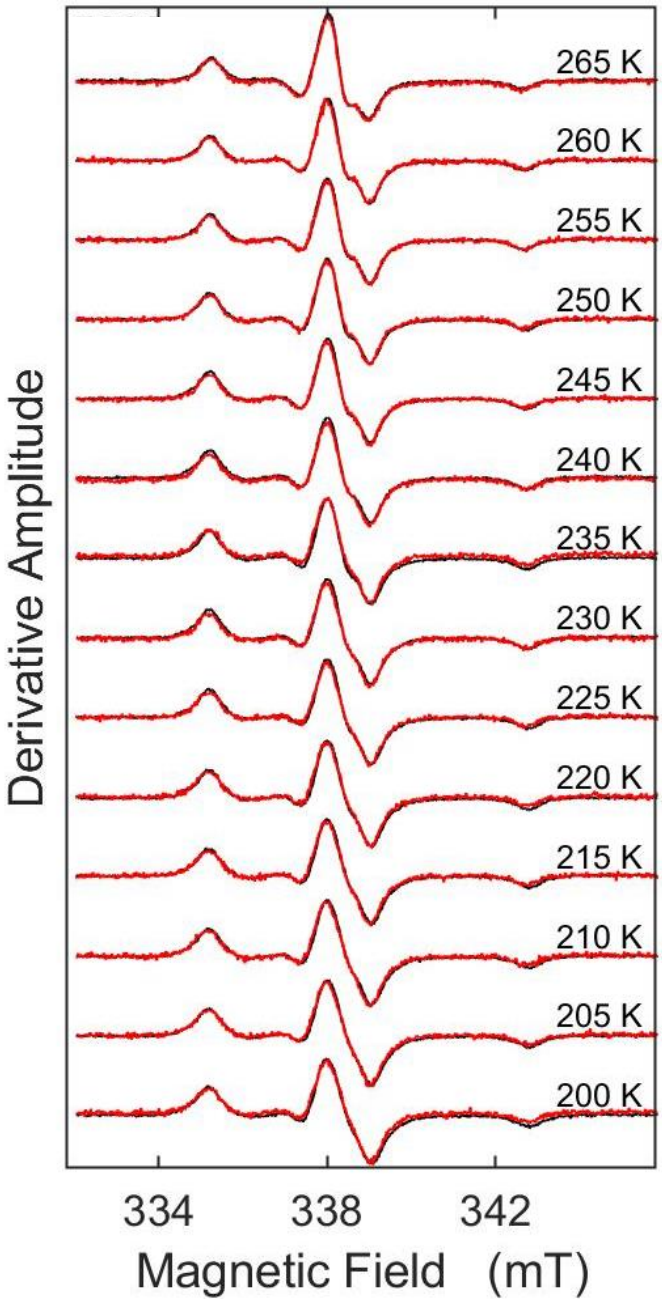


*Figure 4.* Temperature dependence of TEMPOL EPR line shape in frozen solution containing only EGCG. Spectra show rigid-limit, immobile TEMPOL EPR line shape for increasing (black) and decreasing (red) directions of sequential temperature changes over the entire temperature range. Spectra are normalized to the central peak-to-trough amplitude.

**2. Temperature dependence of TEMPOL EPR line shape in frozen $\alpha$-Syn solution in the presence of varying concentrations of EGCG**

Figure 5 shows representative EPR spectra from over the range of temperatures, 200-265 K, for samples that include a-Syn only,[50] and $\alpha$-Syn in the presence of five different concentrations of EGCG. The a-Syn concentration is the same in all samples, and the concentrations of EGCG correspond to EGCG:$\alpha$ -Syn ratios of 1:1, 7:1, 15:1, 60:1 and 100:1. The spectra are normalized to the peak-to-trough amplitude of the central feature, and overlaid, for comparison of the line shapes. The overlaid spectra indicate similar, a relatively immobile solvent phase, characterized by the TEMPOL rigid-limit line shape, for all EGCG concentrations at low temperatures, $T$ < 225 K. At 230 K, a second feature emerges at 336 mT for $\alpha$-Syn only (Fig. 5, cyan spectra), indicating the emergence of a distinguishable second component. This feature is also observed for the other samples, with a trend that samples containing increasingly larger concentrations of EGCG reveal the second component at increasingly higher temperatures. At higher temperatures, the line shape features of the mobile component are clearly evidenced in other regions of the spectral window and result in mobile spectra with the characteristic three-derivative line shape. Notably, Fig. 5 shows that the introduction of $\alpha$-Syn to the system produces a distinctly different *T*-dependence relative to EGCG alone (Fig. 4). At higher temperatures, none of the $\alpha$-Syn + EGCG samples maintain the rigid-limit EPR line shape observed in the EGCG-only spectra (Fig. 4), and they instead progress into a derivative line shape that narrows at sequentially higher temperatures.

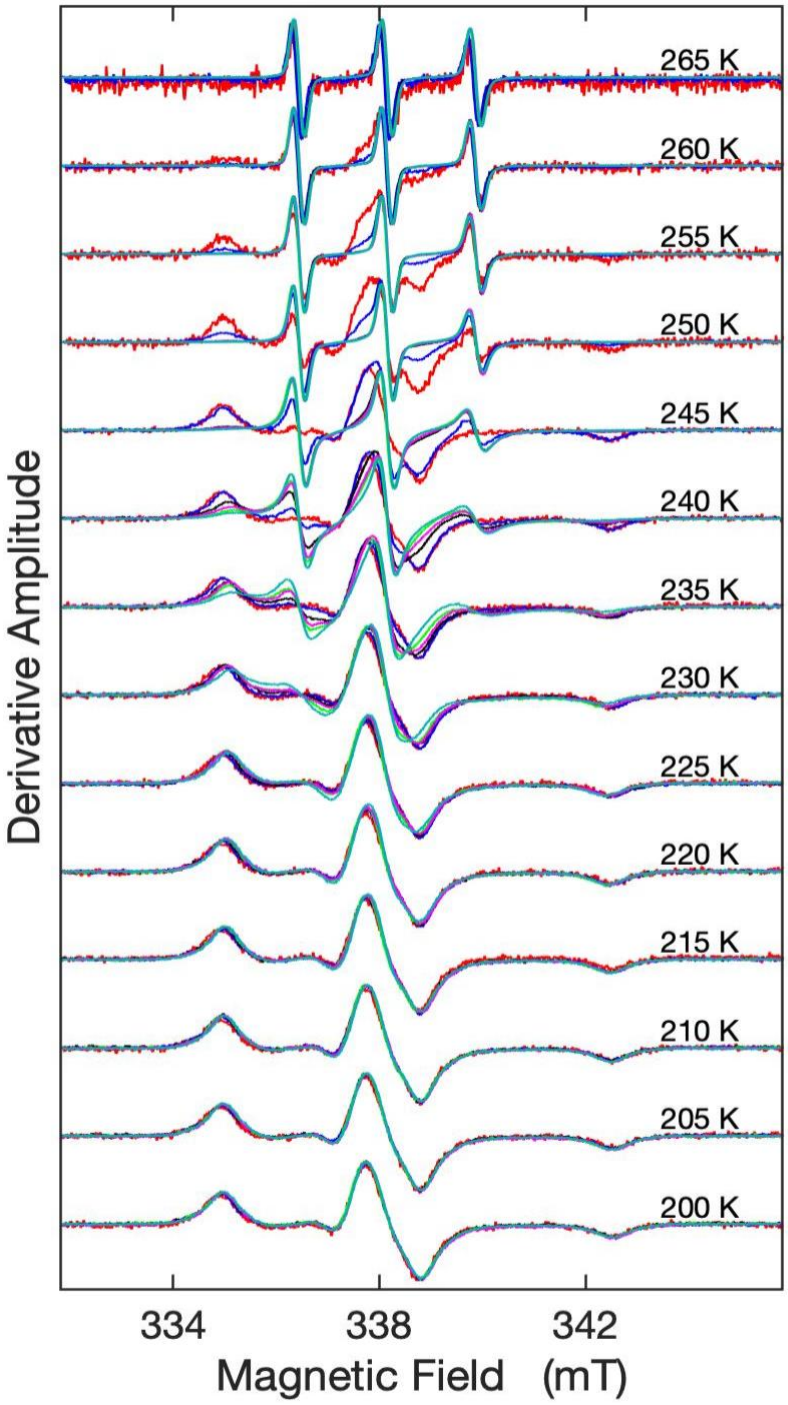


*Figure 5.* Temperature dependence of TEMPOL EPR line shape in frozen solution of $\alpha$-Syn oligomers with varying concentrations of EGCG. Spectra are given for molar ratios of $\alpha$-Syn only (cyan), 1 EGCG: 1 $\alpha$-Syn (green), 7 EGCG: 1 $\alpha$-Syn (magenta), 15 EGCG:1 $\alpha$-Syn (black), 60 EGCG: 1 $\alpha$-Syn (dark blue), and 100 EGCG: 1 $\alpha$-Syn (red). Relatively, spectra show a gradual reduction in mobility as [EGCG] increases relative to [$\alpha$-Syn]. Spectra are normalized to the central peak-to-trough amplitude, and [$\alpha$-Syn] = 34.5 μM for all samples.

**3. Hysteresis in the Temperature dependence of TEMPOL EPR line shape in frozen $\alpha$-syn solution in the presence of varying concentrations of EGCG**

TEMPOL EPR spectra of frozen solution samples of oligomeric $\alpha$-syn in the presence of varied concentrations of EGCG show a shared progression, over the temperature range of 200 – 265 K, from the broad, rigid-limit line shape to a sharp, derivative line shape, with increasing temperature (Fig. 6 - 10).The EPR spectra at EGCG:α-Syn values of 1:1, 7:1, and 15:1 also display a thermal hysteresis in the interval, 235-250 K, dependent upon the direction of *T* change (Figure 6, 7, 8). Spectra within the hysteresis *T* range indicate lower mobility for the spin probe (broader line shape) when measured for increasing *T*, relative to the spectra at the same *T* value, measured in the direction of decreasing *T*. This thermal hysteresis was previously observed for oligomers and fibrils of α-Syn in the absence of EGCG.[50] There does not appear to be a significant effect of [EGCG] on the degree of hysteresis observed. For the 100:1 and 60:1 conditions, loss of the TEMPOL spectral amplitude prevented observation of thermal hysteresis at these concentrations.

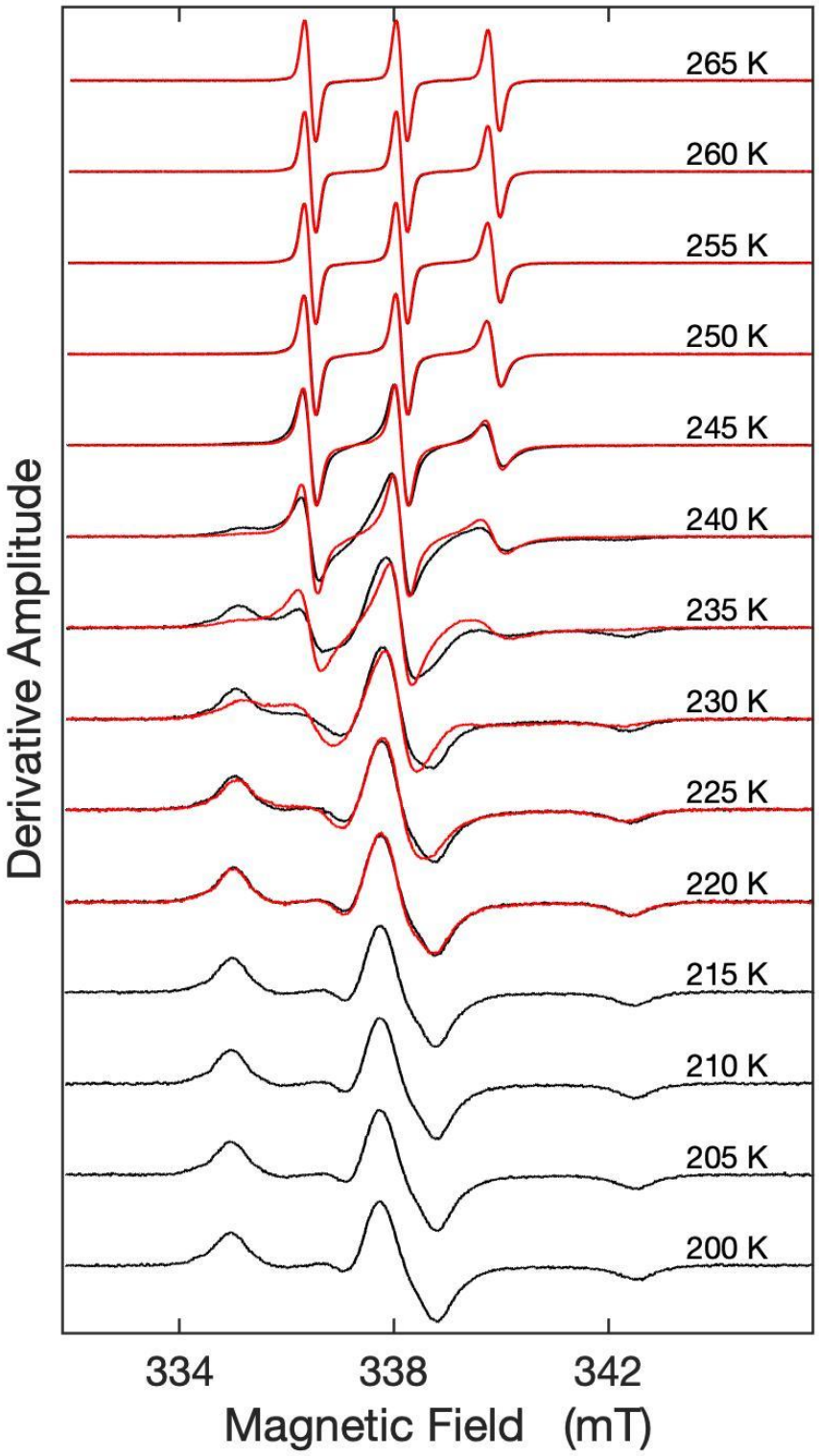


*Figure 6.* Directional *T*-dependence of TEMPOL EPR line shape for frozen $\alpha$-syn solution in the presence of molar ratio of 1:1 EGCG to $\alpha$-syn. Spectra show thermal hysteresis between increasing temperature (black) and decreasing temperature (red) spectra. Spectra are normalized to the central peak-to-trough amplitude.

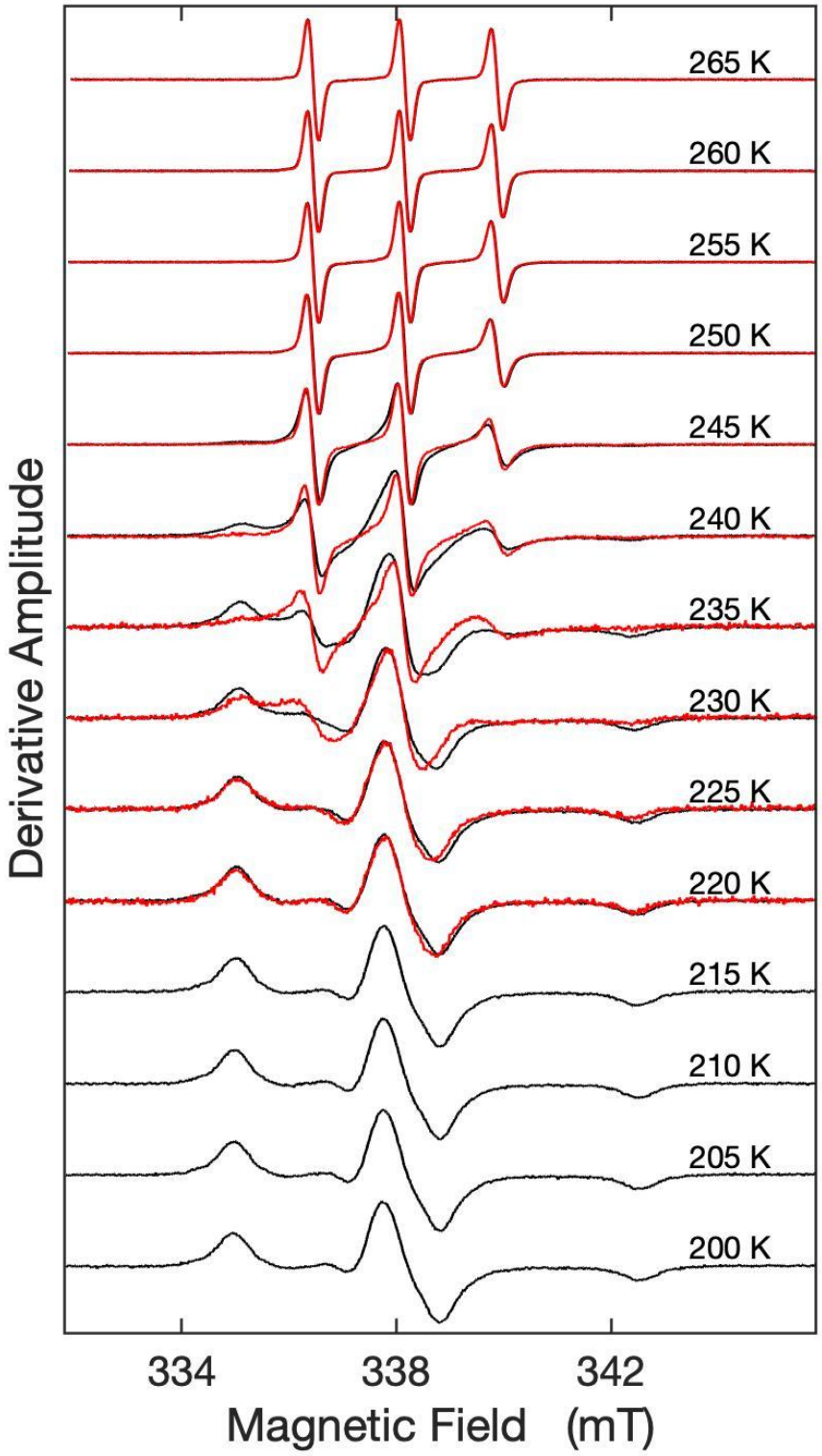


*Figure 7.* Directional *T*-dependence of TEMPOL EPR line shape for frozen $\alpha$-syn solution in the presence of molar ratio of 7:1 EGCG to $\alpha$-syn. Spectra show thermal hysteresis between increasing temperature (black) and decreasing temperature (red) spectra. Spectra are normalized to the central peak-to-trough amplitude.

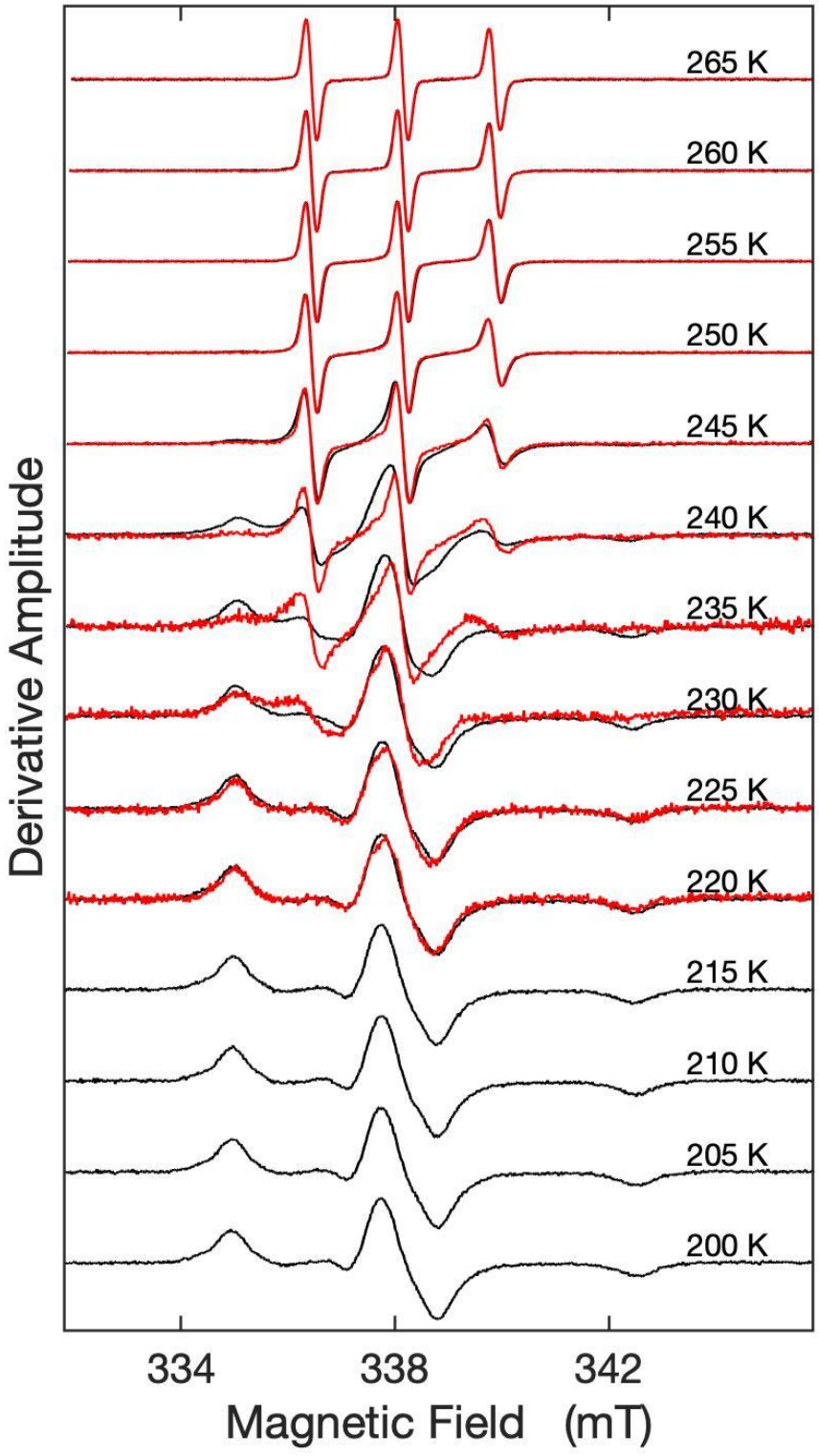


*Figure 8.* Directional *T*-dependence of TEMPOL EPR line shape for frozen $\alpha$-syn solution in the presence of molar ratio of 15:1 EGCG to $\alpha$-syn. Spectra show thermal hysteresis between increasing temperature (black) and decreasing temperature (red) spectra. Spectra are normalized to the central peak-to-trough amplitude. Appearance of noise in the spectra suggests possible loss of TEMPOL radical signal.

**4. Redox reaction at elevated EGCG:α-Syn and *T* values leads to TEMPOL radical annihilation**

The EPR spectra for EGCG:α-Syn values of 60:1 and 100:1 display a prominent loss of the TEMPOL spectral amplitude during spectrum acquisition in the high *T* range (Fig. 9, 10). During the initial spectrum acquisition, which occurs in the direction of increasing *T*, from the base value of 220 K, TEMPOL spectra were obtained with the expected amplitudes. However, upon commencement of the decreasing *T* acquisition, starting from 265 K and continuing through 250 K, the spectra displayed a dramatic decrease in amplitude. The residual amplitude at 250 K is estimated as ~10% and ~1% for the 60:1 and 100:1 EGCG:α-Syn conditions, respectively, based on comparison of the signal-to-noise ratios in the central peak-to-trough normalized spectra. There is some apparent loss of signal amplitude for decreasing-*T* spectra in the 15:1 condition, though it is much less pronounced than at higher [EGCG] (Fig. 8). The quenching of the TEMPOL radical signal does not occur in frozen solution that contains EGCG in the absence of α-Syn (Fig. 4). Quenching of the TEMPOL EPR signal still occurs, to the same extent, in anaerobic samples (data not shown). TEMPOL quenching has not been previously observed for a wide range of proteins and peptides in the frozen solution system (Li et al., PCCP 2022). These results suggest that EGCG undergoes a redox reaction with an amino acid side chain of α-Syn, that produces a free radical species capable of reducing the TEMPOL radical to a diamagnetic form.

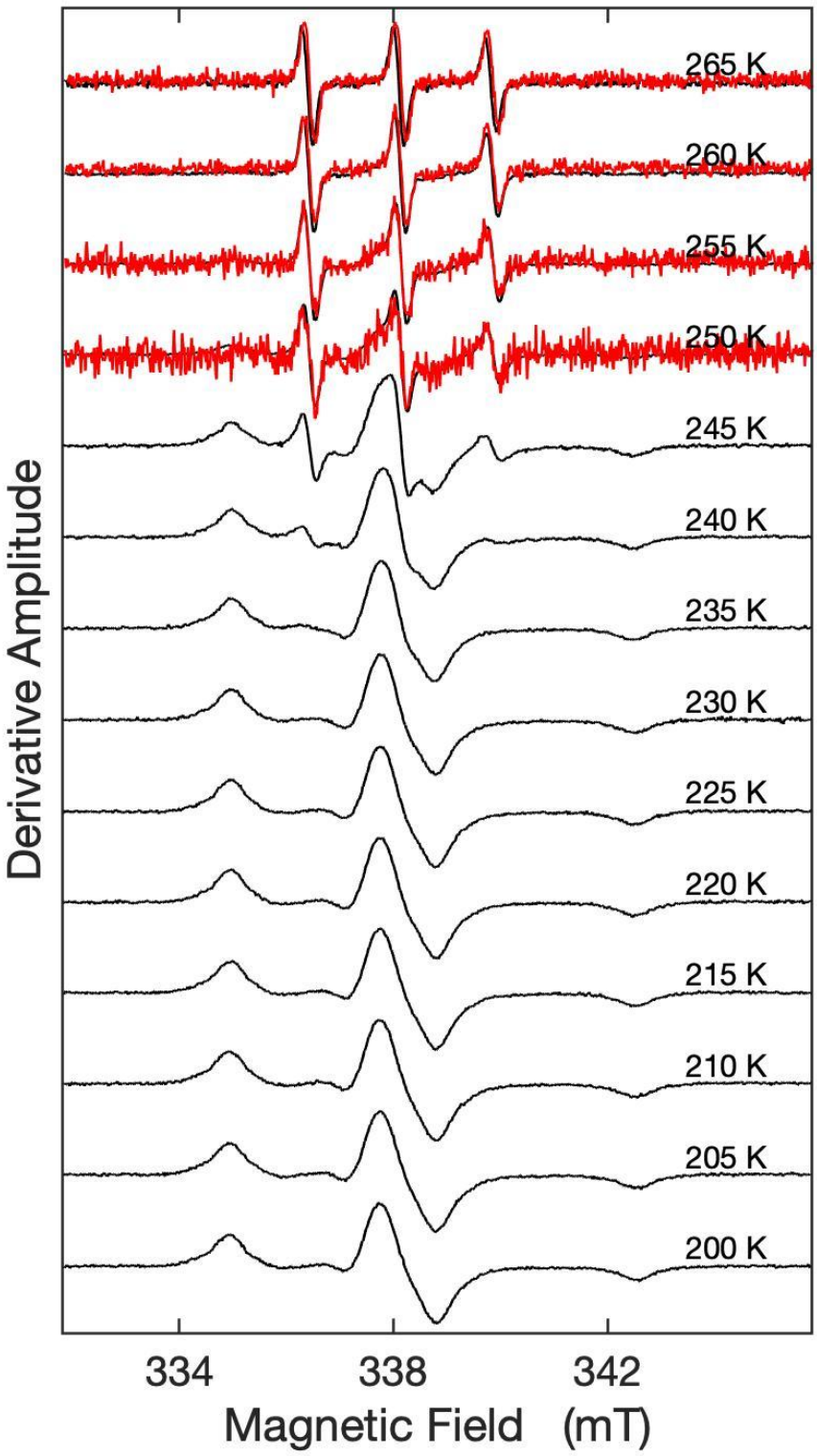


*Figure 9.* Directional *T*-dependence of TEMPOL EPR line shape for frozen $\alpha$-syn solution in the presence of molar ratio of 60:1 EGCG to $\alpha$-syn. Spectra were obtaining first in the order of increasing temperature (black), with spectra acquired in the order of decreasing temperature (red) obtained subsequently. Significant loss of TEMPOL spectral signal amplitude at high *T*, upon commencement of decreasing temperature, prevented observation of thermal hysteresis and suggests the formation of a free radical species.

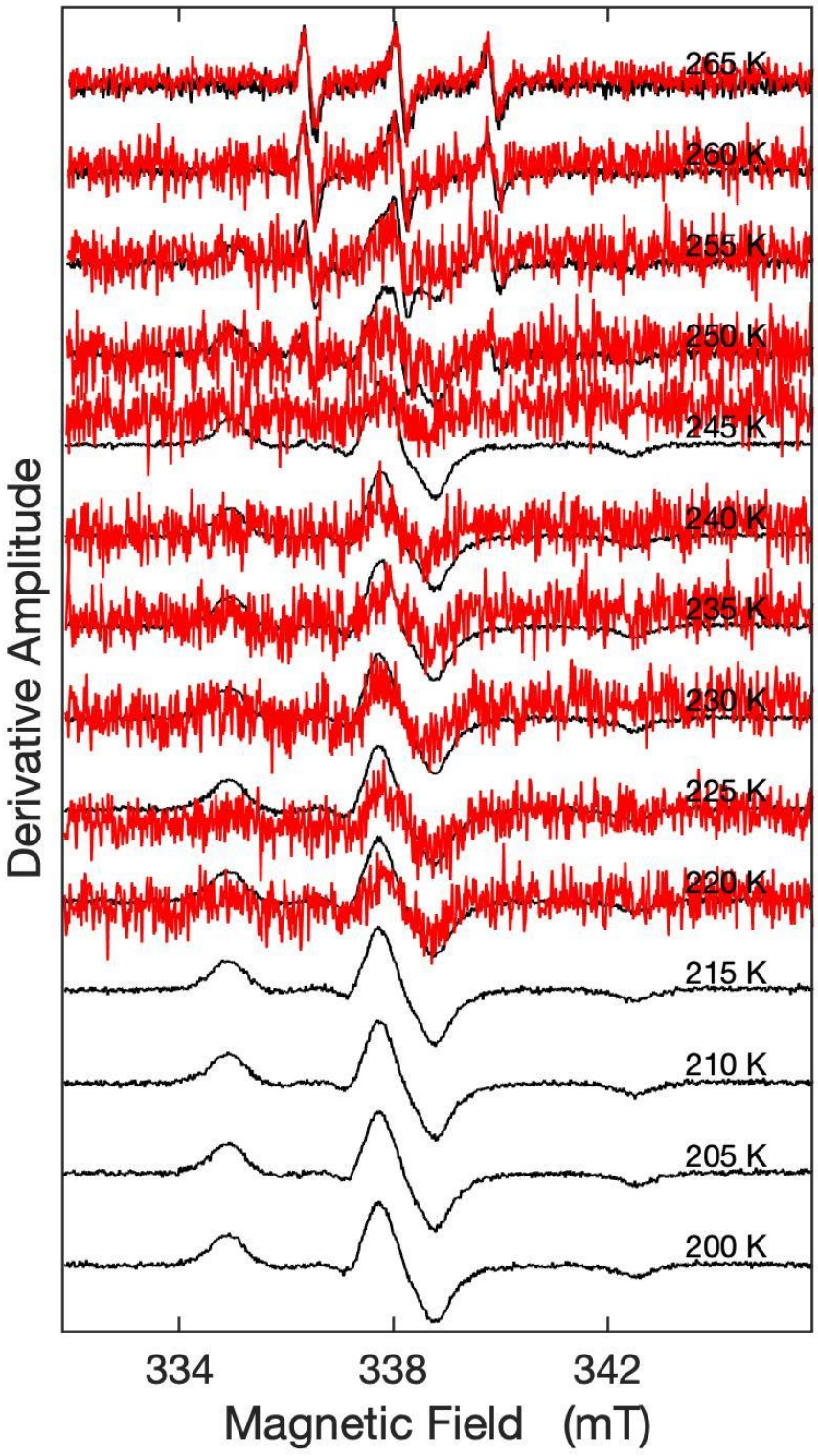


*Figure 10.* Directional *T*-dependence of TEMPOL EPR line shape for frozen $\alpha$-syn solution in the presence of molar ratio of 100:1 EGCG to $\alpha$-syn. Spectra were obtained first in the order of increasing temperature (black), with spectra acquired in the order of decreasing temperature (red) obtained subsequently. Significant loss of TEMPOL spectral signal amplitude at high *T*, upon commencement of decreasing temperature, prevented observation of thermal hysteresis and suggests the formation of a free radical species.

**5. Simulation of the Temperature dependence of the TEMPOL EPR spectra in the presence of varying concentrations of EGCG**

Figures 11 - 15 show the experimental spectra, and overlaid simulations of the EPR spectra, for the EGCG:$\alpha$-Syn ratios of 1:1, 7:1, 15:1, 60:1 and 100:1, respectively. The simulations correspond to the direction of increasing $T$ values, starting from 220 K. The simulations of the α-syn EPR line shapes reveal two mobility components: relatively slow (mobility, $\log \tau_{c,s}$; normalized weight, $W_s$) and fast ($\log \tau_{c,f}$, $W_f$). The weight of the fast component is dominant in high-$T$ range of $T \geq 255$ K. The slow component grows in proportion as the $T$ is lowered, and becomes dominant below 235 K. At sufficiently low temperatures ($T \leq$ 220 K), the spectra show a broad, rigid-limit, single-component line shape, and simulations were not carried out for spectra.

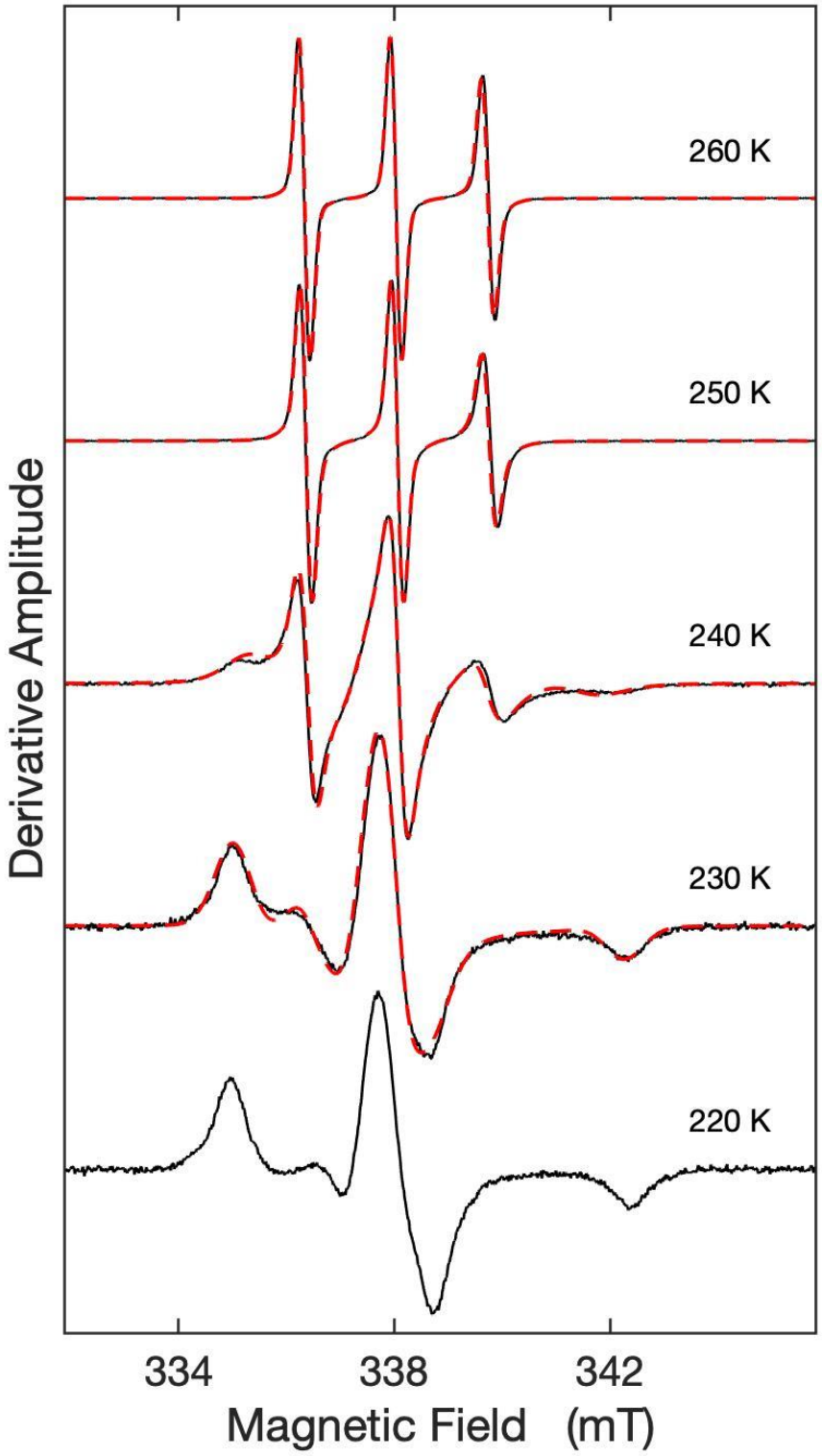


*Figure 11.* Temperature dependence of the TEMPOL EPR spectrum (black) in frozen solution of $\alpha$-Syn oligomers with molar ratio 1:1 EGCG to $\alpha$-syn. Spectra were obtained in the direction of increasing temperature and overlaid with simulated two-component EPR spectra (red, dashed line). Simulations show good agreement with measured spectra. Simulations were not obtained for rigid-limit single-component spectra.

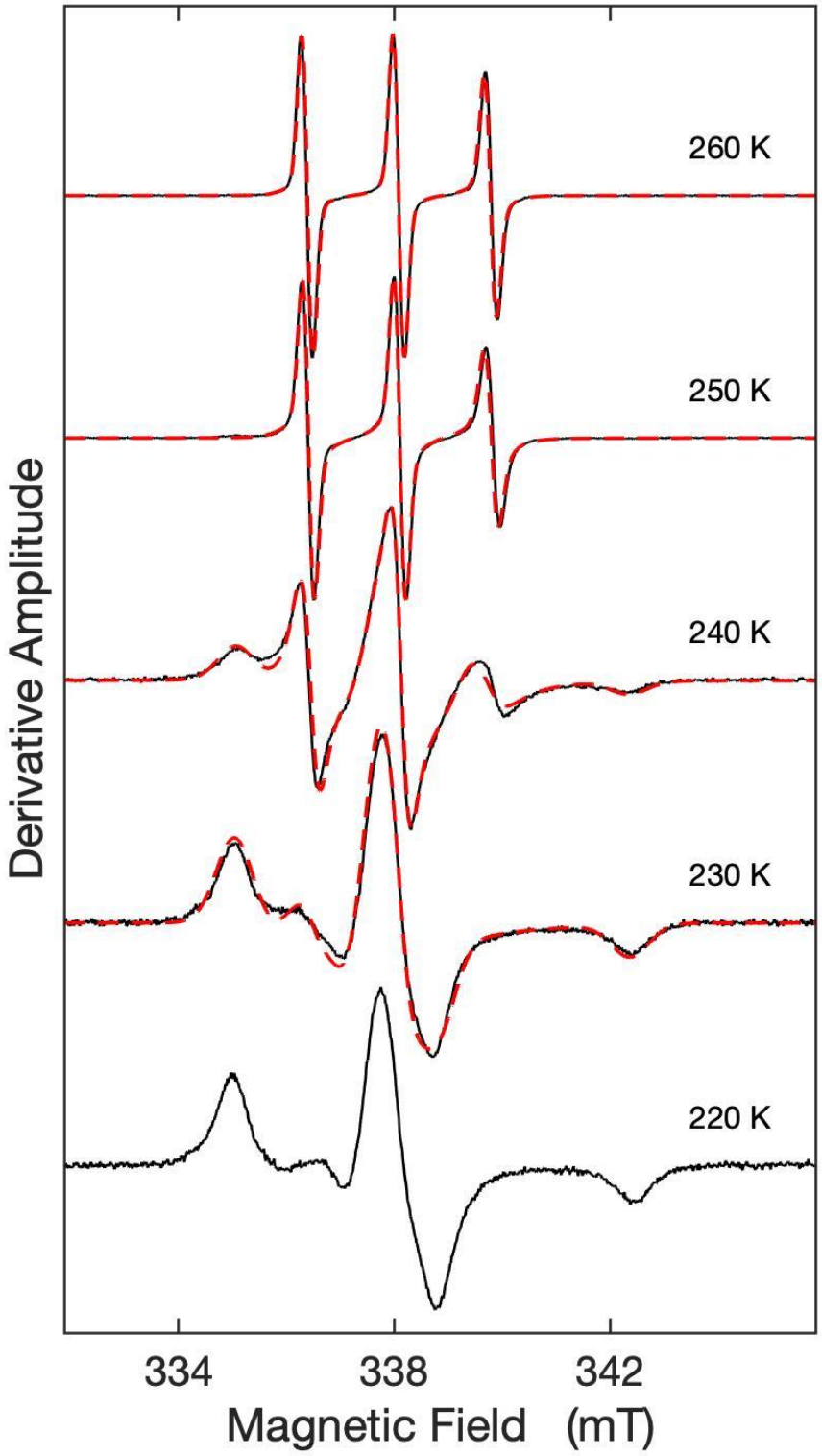


*Figure 12.* Temperature dependence of the TEMPOL EPR spectrum (black) in frozen solution of $\alpha$-Syn oligomers with molar ratio 7:1 EGCG to $\alpha$-syn. Spectra were obtained in the direction of increasing temperature and overlaid with simulated two-component EPR spectra (red, dashed line). Simulations show good agreement with measured spectra. Simulations were not obtained for rigid-limit single-component spectra.

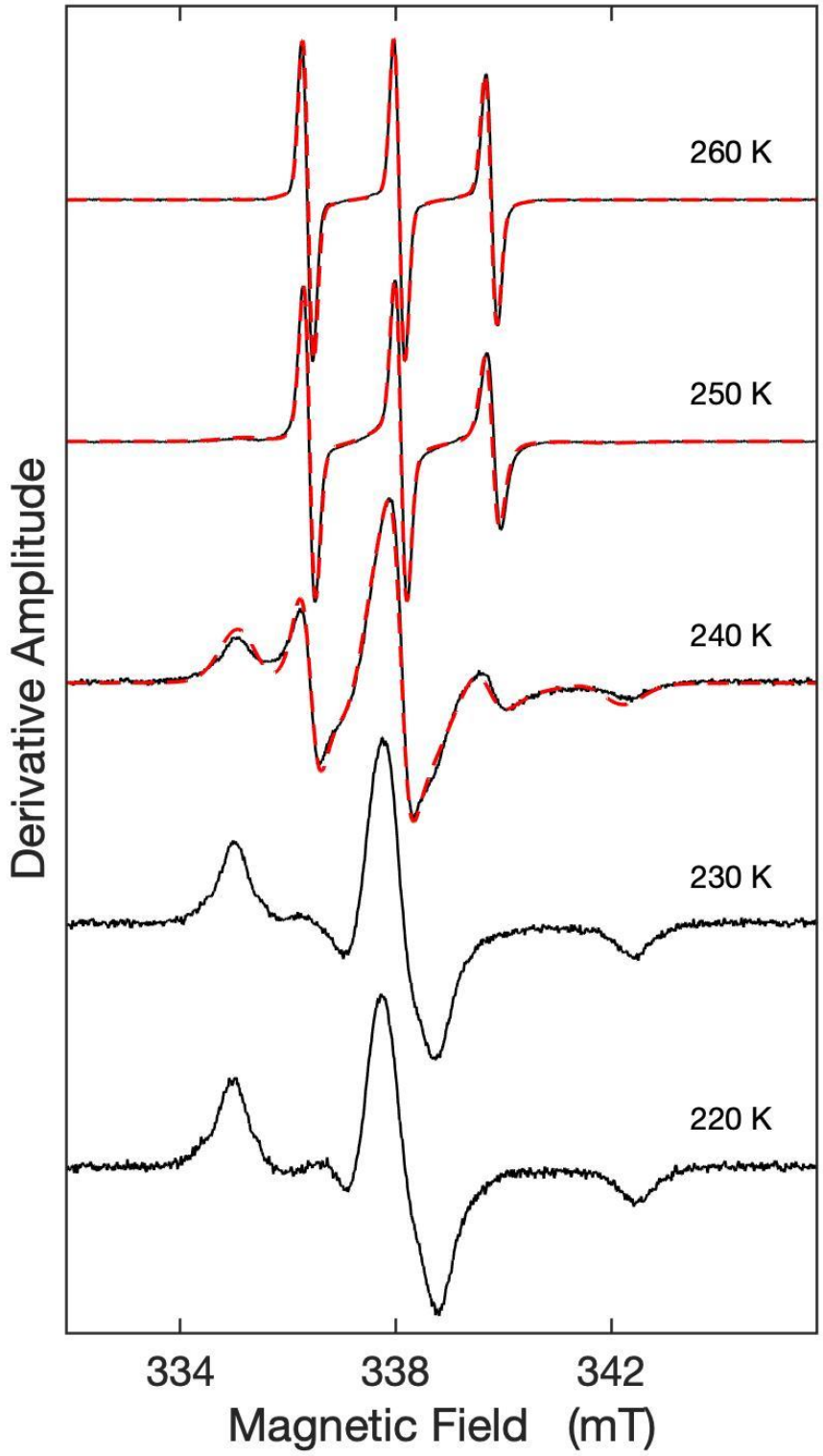


*Figure 13.* Temperature dependence of the TEMPOL EPR spectrum (black) in frozen solution of $\alpha$-Syn oligomers with molar ratio 15:1 EGCG to $\alpha$-syn. Spectra were obtained in the direction of increasing temperature and overlaid with simulated two-component EPR spectra (red, dashed line). Simulations show good agreement with measured spectra. Simulations were not obtained for rigid-limit single-component spectra.

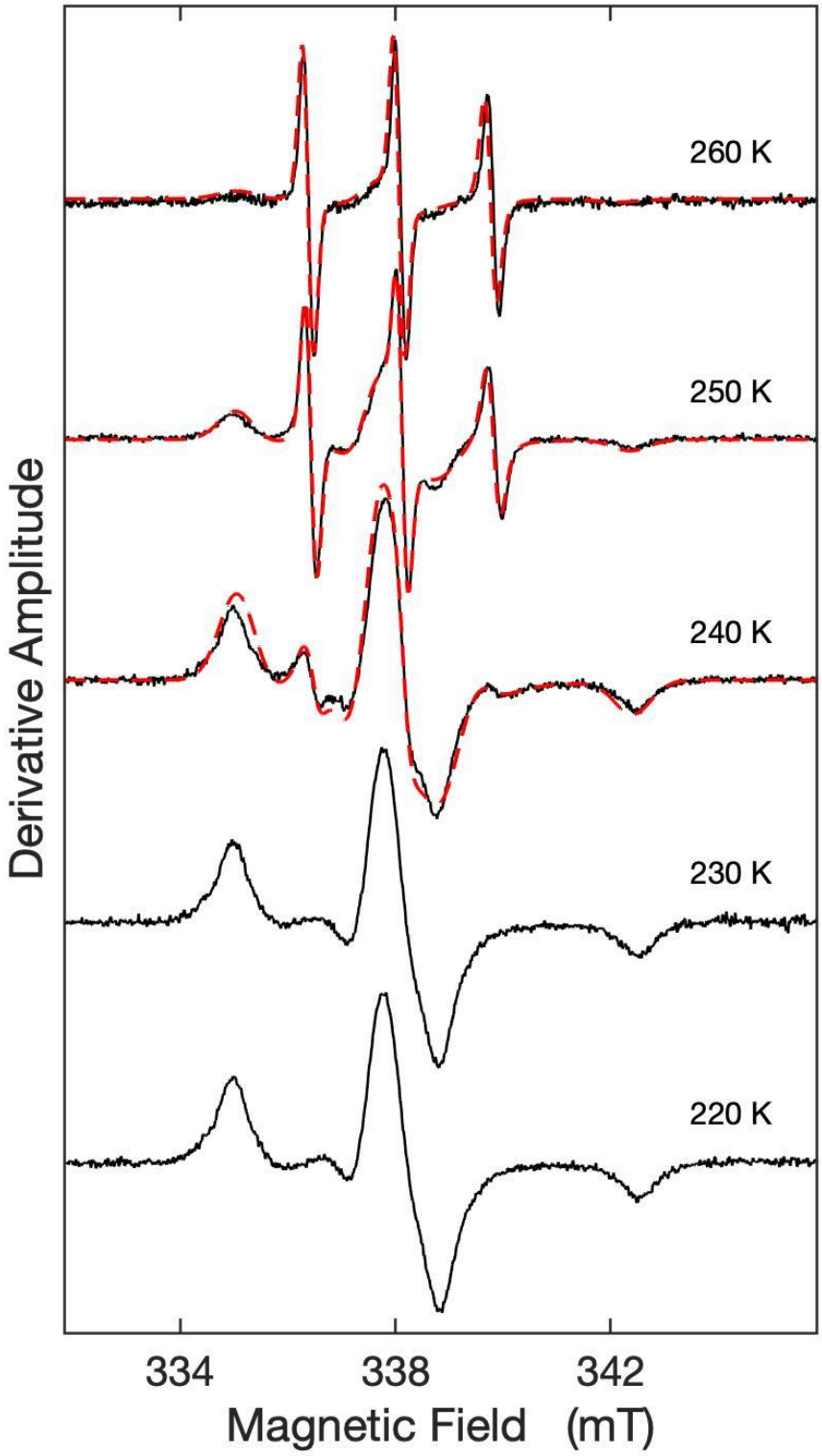


*Figure 14.* Temperature dependence of the TEMPOL EPR spectrum (black) in frozen solution of $\alpha$-Syn oligomers with molar ratio 60:1 EGCG to $\alpha$-syn. Spectra were obtained in the direction of increasing temperature and overlaid with simulated two-component EPR spectra (red, dashed line). Simulations show good agreement with measured spectra. Simulations were not obtained for rigid-limit single-component spectra.

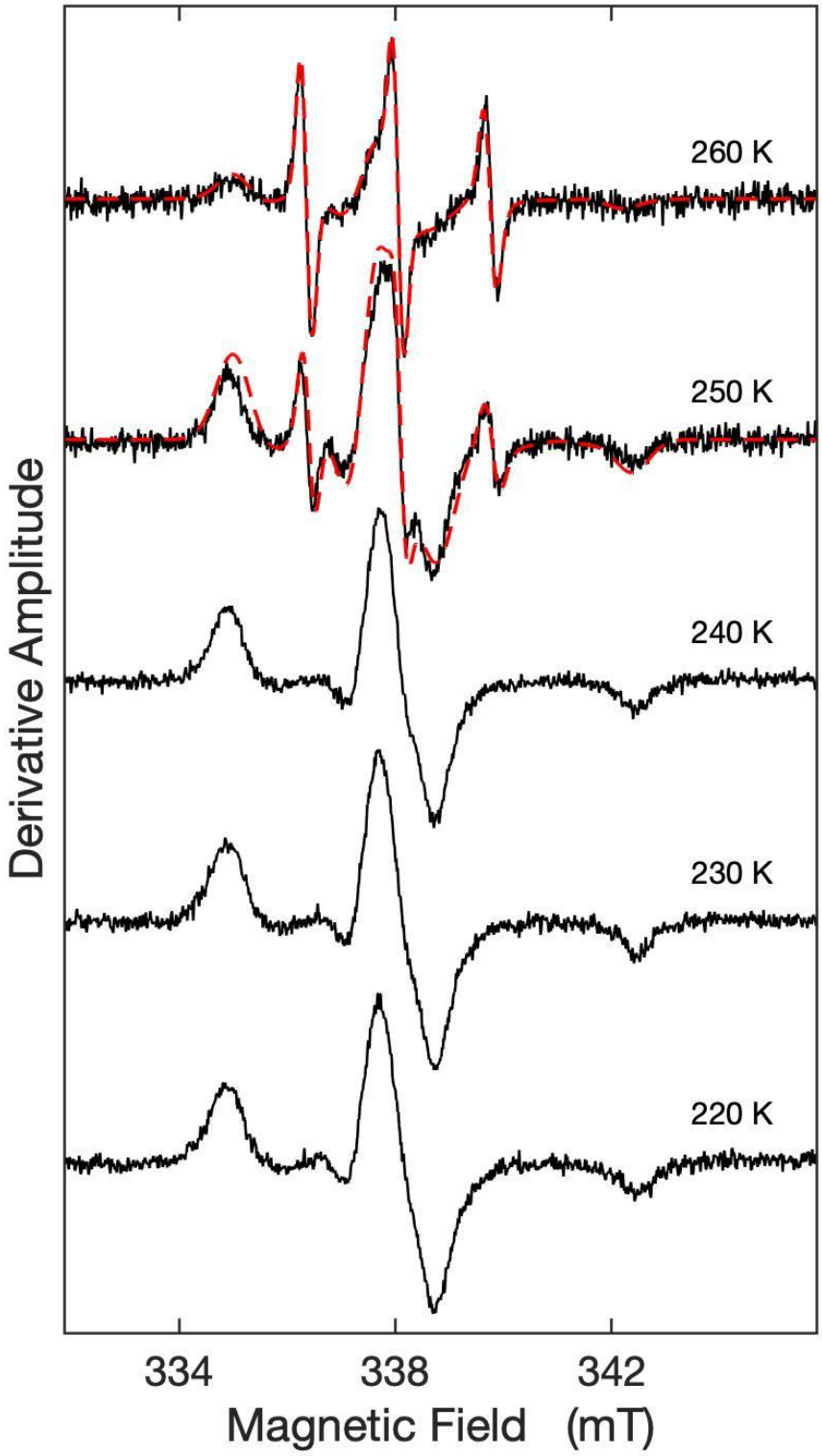


*Figure 15.* Temperature dependence of the TEMPOL EPR spectrum (black) in frozen solution of $\alpha$-Syn oligomers with molar ratio 100:1 EGCG to $\alpha$-syn. Spectra were obtained in the direction of increasing temperature and overlaid with simulated two-component EPR spectra (red, dashed line). Simulations show good agreement with measured spectra. Simulations were not obtained for rigid-limit single-component spectra.

**6. Temperature dependence of TEMPOL rotational correlation times and normalized component weights under varying EGCG concentrations.**

Figure 16 shows the temperature dependence of TEMPOL rotational correlation times and normalized mobility component weights for $\alpha$-Syn samples containing varying concentrations of EGCG. Simulations of the $\alpha$-Syn[50] and $\alpha$-Syn + EGCG line shapes reveal two mobility components: a relatively fast component (mobility, $\log \tau_{C,\mathrm{f}}$, normalized weight, $W_\mathrm{f}$), and a slow component (mobility, $\log \tau_{C,\mathrm{s}}$, normalized weight, $W_\mathrm{s}$). The T-dependence follows the same overall trend for each concentration, with the weight of the slow component dominating over the low temperature range, and the weight of the fast component becoming dominant as T is raised (Fig. 16B). The crossover temperature is defined as the temperature at which $W_\mathrm{f}$ and $W_\mathrm{s}$ are equal. Above the crossover temperature the weight of the fast component becomes dominant. Over the range of EGCG concentrations, a trend emerges, such that the weight of the slow component remains dominant through increasingly higher temperatures as [EGCG] is increased relative to [$\alpha$-Syn]. In contrast, the crossover temperature approaches that of $\alpha$-Syn oligomers as [EGCG] is lowered (Fig. 16B). Additionally, the slow component becomes relatively less mobile as [EGCG] is increased relative to [$\alpha$-Syn], as indicated by the increasing $\log \tau_{C,\mathrm{s}}$ (Fig. 16A). In contrast, the fast components over the entire concentration range follow approximately the same T-dependence as for $\alpha$-Syn alone, with $\log \tau_{C,\mathrm{f}}$ values for all samples approximately aligned throughout the range of temperatures (Fig. 16A). At low [EGCG] (1:1 and 7:1), the *T*-dependence of $\log\tau_{C,\mathrm{s}}$ is comparable to that of $\alpha$-syn only (Fig. 12A) as well. A transition seems to occur between the low [EGCG] conditions and high [EGCG] conditions (60:1 and 100:1) such that the slow component becomes immobilized at higher *T* in high [EGCG]

samples. There is also a transition in that the *T*-dependences of the component weights follow different trajectories in the high [EGCG] treatment, compared to the low [EGCG] conditions (Fig. 16B). The component weights for the 15:1 condition display an intermediate *T*-dependence between the trajectories of low [EGCG] and high [EGCG]. The greatest [EGCG]-dependent shifts in crossover temperature occur between $\alpha$-syn only and 1:1 $\alpha$-syn:EGCG, and 15:1 to 60:1 $\alpha$-syn:EGCG (Fig. 16B).

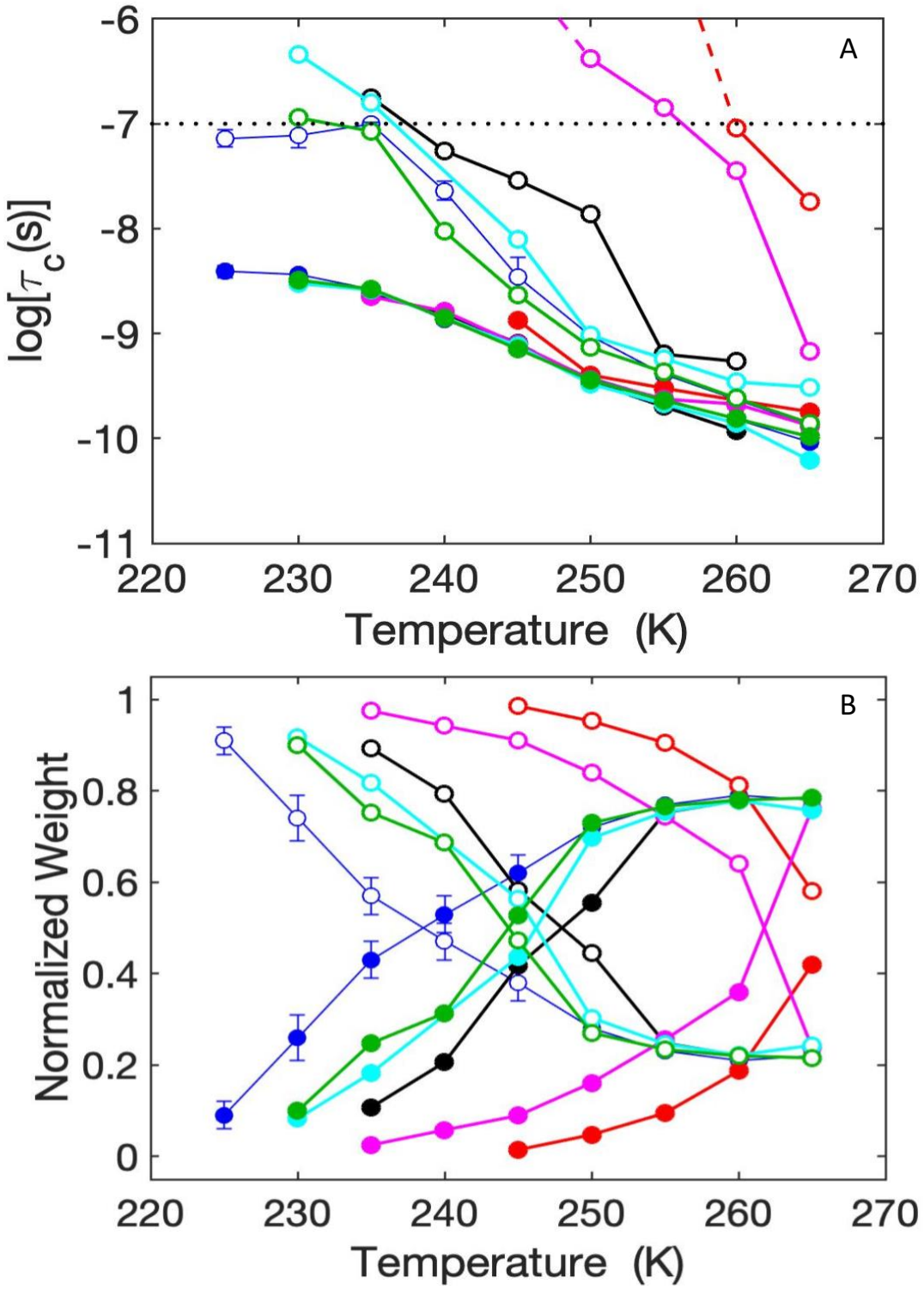


*Figure 16.* Temperature dependence of the rotational correlation time of TEMPOL and normalized mobility component weights of frozen $\alpha$-Syn solutions containing varying concentrations of EGCG. (A) Log $\tau_C$ values for $\alpha$-Syn only (blue), 1:1 EGCG to $\alpha$-Syn (green), 7:1 EGCG to $\alpha$-Syn (cyan), 15:1 EGCG to $\alpha$-Syn (black), 60:1 EGCG to $\alpha$-Syn (magenta), and 100:1 EGCG to $\alpha$-Syn (red). (B) W (normalized component weight) values for $\alpha$-Syn + EGCG samples with same color code as for panel A. In each panel, solid symbols represent the fast components (Log $\tau_{C,f}$, $W_f$), or single components for each concentration, and open symbols represent the slow components ((Log $\tau_{C,s}$, $W_s$). The horizontal dashed line in (A) represents the upper limit for detection of TEMPOL tumbling motion. Error bars represent standard deviations for 3 separate determinations.[50] [$\alpha$-Syn] = 34.5 µM for all samples.

**7. TEM of aqueous $\alpha$-Syn + EGCG samples.**

TEM of oligomeric $\alpha$-syn EPR samples, which were prepared from a lyophilized powder and subsequently cryotrapped, reveal a species with an average diameter of 10-20 nm (Fig. 17A). These smaller structures seem to form aggregates that can reach approximately 100 nm in length. $\alpha$-Syn similarly prepared from a lyophilized powder revealed features with comparable sizes (10-90 nm) and shapes, which were assigned as oligomers.[27]

Addition of 100:1 M EGCG shows a species with slightly differing morphology. The observed species is more circular, with a well-defined boundary (Fig. 17B) compared to oligomers formed from $\alpha$-syn only. The species observed in the presence of EGCG is also slightly smaller, with a mean diameter of 10-15 nm (Fig. 17B). This species also appears to form aggregates, though these larger features reach only about 50 nm in length, and their components largely retain the punctate circular structures of their non-aggregated form.

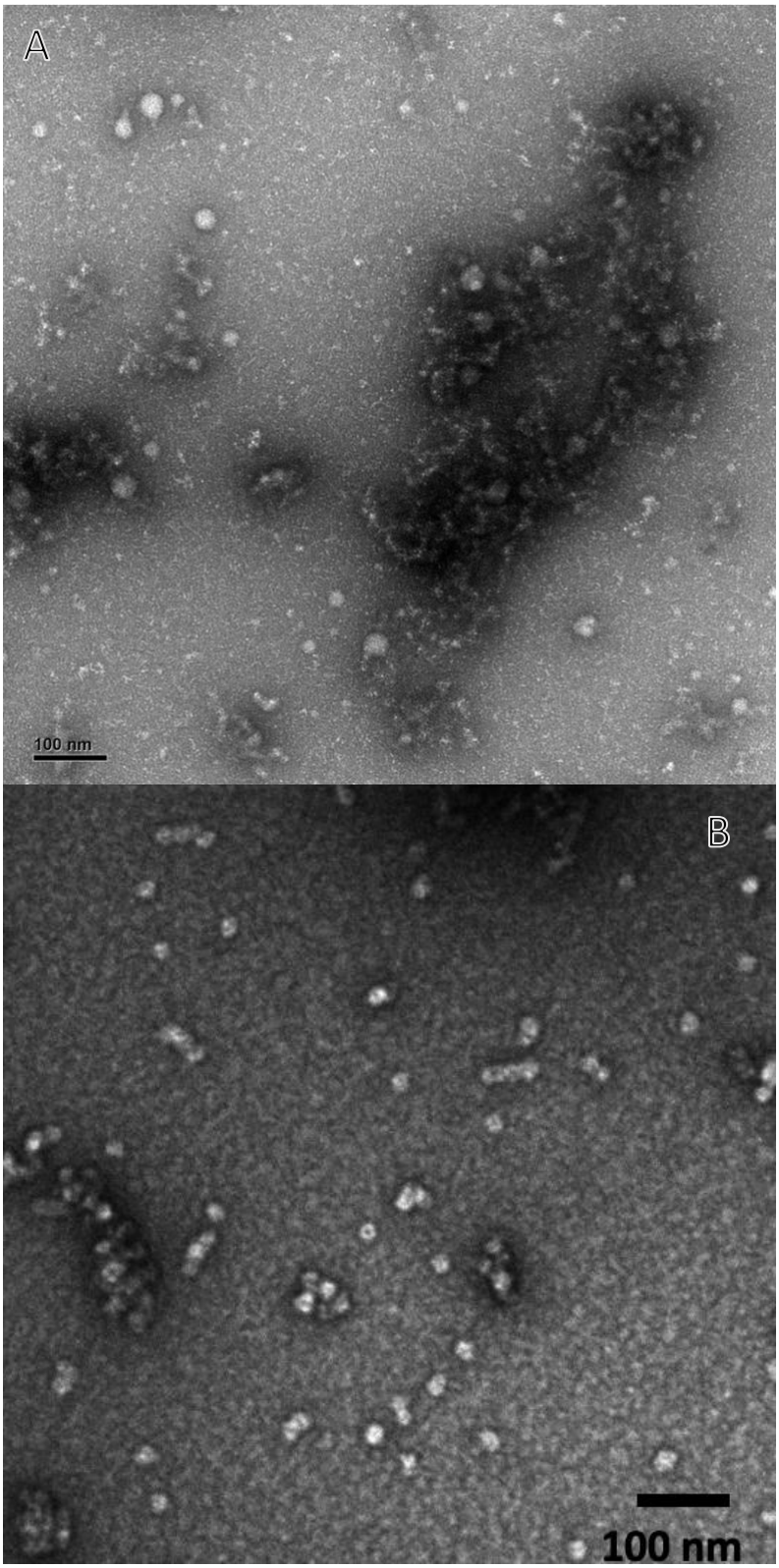


*Figure 17.* Transmission electron micrographs of oligomeric $\alpha$-syn from EPR samples. (A) $\alpha$-syn oligomers only; and (B) $\alpha$-syn oligomers in presence of 100:1 molar ratio of EGCG to $\alpha$-syn. Scale bar, 100 nm.

## Discussion

### 1. Confirmation of oligomeric α-syn by TEM

Our preparatory method of cryotrapping, and our observed TEM features (Fig. 17A) for $\alpha$-syn in the absence of EGCG (Whitcomb & Warncke, 2023), are in agreement with those of lyophilized samples of oligomeric $\alpha$-syn which have been structurally characterized by cryo-EM.[27] Therefore, the aggregate species observed in our EPR samples are $\alpha$-syn oligomers. Preliminary findings from TEM of $\alpha$-syn in the presence of a 100:1 ratio of EGCG show smaller, punctate oligomers, that are characteristic of $\alpha$-syn in the presence of high concentrations of EGCG.[29] Preliminary TEM of $\alpha$-syn in the presence of varying concentrations of EGCG (not shown) suggest that the oligomer morphology at low ratios of EGCG to $\alpha$-syn (0.6:1, 6:1) closely resembles $\alpha$-syn oligomers in the absence of EGCG. These results suggest that there is a transition in global EGCG-oligomer interactions between the low EGCG/$\alpha$-syn ratios (1:1, 7:1, 15:1) and the high ratios (60:1, 100:1) that are examined here.

### 2. Analysis of temperature dependence of TEMPOL EPR line shape in frozen EGCG solution sample

EPR spectra of TEMPOL in frozen solution containing EGCG over the temperature range 200 – 265 K show a persistent, rigid-limit, broad line shape (Fig. 4). There is thus no distinguishable second mobility component. The EPR spectrum is not broadened or distorted, as observed when TEMPOL is frozen in aqueous solution in the absence of a glass-forming, aqueous-cryosolvent.[42] These findings suggest EGCG forms a glassy interstitial phase in frozen

aqueous solution, effectively sequestering and immobilizing TEMPOL. Such a result is consistent with the reported glass transition temperature ($T_g$) of EGCG, which lies well above the temperature range of our experiments; for solid amorphous EGCG prepared by lyophilization of pure aqueous solution, $T_g$ was found to be 163˚C (436 K).[52] It is therefore likely that the freeze-concentrated EGCG in our system forms an immobile, glass-like phase over the experimental temperature range.

### 3. Concentration-dependent effects of EGCG on temperature dependence of TEMPOL EPR line shape in frozen aqueous α-syn solutions

The temperature dependence of the TEMPOL EPR line shape in frozen aqueous $\alpha$-syn solutions is modulated in a concentration dependent manner by EGCG. That is, features of the TEMPOL line shape vary for a given temperature, depending on the concentration of EGCG present. The first of these concentration-dependent features is the persistence of the low-temperature, rigid-limit mobility component as the temperature is raised to higher values. Compared to the rigid-limit spectra of EGCG-only (Fig. 4), the $\alpha$-syn-containing samples consistently show a shift from rigid-limit TEMPOL line shape to a tri-derivative line shape as temperature is increased (Fig. 5). However, for increasingly higher concentrations of EGCG, the characteristic low-field peak of the broad, rigid-limit TEMPOL line shape does persist to higher temperatures. For molar ratios of 1:60 and 1:100 $\alpha$-syn to EGCG, this low-field peak persists clearly up to 255 K and 260 K, respectively, whereas this feature disappears for $T \geq 230$ K for $\alpha$-

syn alone and $T \geq 235$ K for a 1:1 molar ratio (Fig. 5). Andersen et al. reported binding of EGCG occurred at a ratio of approximately 54:1 EGCG per $\alpha$-syn in EGCG-induced oligomers and ~7:1 EGCG per $\alpha$-syn when added to preformed oligomers.[29] Thus, at molar ratios greater than 54:1 EGCG:$\alpha$-syn, some EGCG should be free in solution. We observed that EPR measurements of TEMPOL for EGCG-only in the ice-confined mesodomain system produces consistent broad, rigid-limit spectra. If the free EGCG in solution is unperturbed by or sequestered from $\alpha$-syn, it should still produce this EPR line shape. It is unsurprising then that a rigid, immobile component is more pronounced and persists to higher temperatures for higher [EGCG] samples.

The EPR spectra of TEMPOL in frozen aqueous oligomeric $\alpha$-syn solution samples in the presence of varied EGCG concentrations show an [EGCG]-dependent gradient of mobilities. Temperatures in the middle of our experimental range (235 K $\leq T \leq$ 240 K) clearly illustrate the heterogeneity in protein-coupled solvent mobility, depending on [EGCG] (Fig. 5). Beyond the persistence of an immobile slow component, increasing [EGCG] corresponds to reduced TEMPOL mobility, which is reflected in the stepwise broadening of the low-field features of the TEMPOL derivative line shape with increasingly concentrated EGCG (Fig. 5). From inspection, this trend holds for all concentrations of EGCG tested, and thus, EGCG exhibits an attenuating effect on $\alpha$-syn mobility even at a 1:1 ratio. Calcein release assays have demonstrated that EGCG inhibits the ability of $\alpha$-syn oligomers to permeabilize membranes in dose-response fashion, with an observed effect at a 1:1 ratio.[32] Additionally, the NTD of $\alpha$-syn is reportedly crucial for membrane association and permeabilization,[53] a highly dynamic NTD is associated with increased cytotoxicity and membrane permeabilization,[33] and EGCG has been shown to stabilize and reduce the mobility of the NTD in $\alpha$-syn oligomers,[29] particularly residues 5-17.[18]

Our findings are thus consistent with these data, indicating that EGCG attenuates $\alpha$-syn dynamics, purportedly by association with and stabilization of the NTD and NAC regions.

**4. Redox reaction of EGCG and $\alpha$-syn leads to TEMPOL radical annihilation**

Interestingly, EGCG concentration also appears to affect the EPR spectral amplitude of TEMPOL. As temperature is increased, the TEMPOL EPR signal begins to degrade, yet this phenomenon is most pronounced in samples containing high [EGCG], such as the 100:1 and 60:1 samples (Fig. 9, 10) and is not as apparent in low [EGCG] samples, such as the 1:1 sample (Fig. 6). Thus, an increasing diminishment of TEMPOL EPR signal is correlated with increasing [EGCG]. EGCG is a known radical scavenger and antioxidant,[34] so it is plausible that EGCG could eradicate the unpaired spin of TEMPOL via a redox mechanism. However, this marked reduction in TEMPOL EPR signal is not observed for EGCG-only samples, indicating that EGCG alone is not responsible for the loss of signal amplitude. The same loss of TEMPOL EPR signal occurs under anaerobic conditions (data not shown), which indicates that dioxygen, and derived superoxo- or peroxyl radical species, are not involved. Annihilation of the TEMPOL unpaired electron by a free radical species may provide an explanation for this signal degradation. Taken together, these findings suggest that a redox reaction takes places between $\alpha$-syn and EGCG, producing a free radical species capable of annihilating the nitroxide radical of TEMPOL. Grønnemose et al. (2022) reported slight oxidation of $\alpha$-syn oligomers treated with EGCG but saw substantial oxidation of oligomers formed in the presence of EGCG.[18] Thus, saturating oligomeric $\alpha$-syn solution samples, which inevitably includes some monomeric protein, could plausibly produce a redox reaction by which EGCG oxidizes $\alpha$-syn. Previous studies employing hydrogen-deuterium exchange mass spectroscopy,[18] and water-saturation

transfer difference heteronuclear single-quantum coherence experiments,[54] reported EGCG reduces solvent exposure, exerting a protective, stabilizing effect, in oligomeric $\alpha$-syn and A$\beta$40. Yet this protective effect was abrogated in EGCG-induced $\alpha$-syn oligomers for which Met residues within the NTD were oxidized.[18] The TEMPOL annihilation may thus arise from EGCG reaction with one or more of the four Met residues in $\alpha$-syn, to produce a free radical species.

**5. Analysis of temperature dependence of TEMPOL rotational correlation times and normalized component weights under varying EGCG concentrations**

Temperature dependence of the simulation parameters, $\tau_c$ and *W*, in the presence of varied [EGCG] reflects the concentration-dependent effects on TEMPOL line shape (Fig. 16). The use of simulation parameters allows for these effects to be quantified, relative to the analysis of the EPR line shapes (Fig. 5, 11-15). Notably, $\tau_{c,\mathrm{f}}$ is comparable across the entire range of [EGCG] studied, which indicates that a fraction of the mesophase retains the native dynamical character and fluidity of $\alpha$-syn in the mesodomain system, independent of [EGCG]. It is therefore most likely that, on the time scales of our experiment, EGCG associates most with the less mobile, NTD/NAC "core" of the oligomers, and the highly mobile IDRs retain their dynamics. Our findings are consistent with this scenario and are similarly corroborated by reports that EGCG immobilizes the NTD on a time scale of ~2 hrs. and immobilizes the CTD on a time scale of several days.[29]

Comparatively, the [EGCG] dependence is observed only in the slow component rotational mobilities, $\tau_{c,s}$ (Fig. 16A). The slow components corroborate the gradient of mobilities

and dose-response relationship between [EGCG] and rotational mobility observed directly from the overlaid spectra in Fig. 5 such that the *T*-dependence curves for the slow component at each concentration approach that of $\alpha$-syn-only as [EGCG] goes to 0. At low [EGCG] (1:1 and 7:1), the *T*-dependence of $\log\tau_{c,s}$ is comparable to that of $\alpha$-syn-only (Fig. 16A). The $\tau_{c,s}$ values for varied EGCG concentrations also support the notion of a persistent, immobile component as they reach the rigid limit for detection ($\tau_c > 10^{-7}$ s) at increasingly higher temperatures as [EGCG] is increased. These slow components become mobile at sufficiently high temperatures, which suggests that the PAD-like component is not sequestered from $\alpha$-syn, as this would produce the characteristic rigid-limit EPR spectra of EGCG-only.

Fig. 16B reveals [EGCG] dependent effects on the *T*-dependence of the normalized mobility component weights. In general, increasing [EGCG] leads to a relative increase in the proportion of the slow component at a given temperature. The less mobile, PAD-like slow component is associated with increased confinement compared to the fast component mesophase. Thus, addition of EGCG does increase confinement within the system in a concentration dependent manner.

**6. Analysis of directional temperature dependence and thermal hysteresis of the TEMPOL EPR spectrum for frozen α-syn solution in the presence of varying concentrations of EGCG**

Thermal hysteresis was observed between EPR spectra of TEMPOL in frozen oligomeric $\alpha$-syn solution samples in the presence of varied [EGCG], obtained for increasing *T* and decreasing *T*, respectively. For these samples, the EPR spectra at each *T* value, and therefore the hysteresis, are independent of sample holding time.[50] This thermal hysteresis has not been observed in previous spin probe studies of soluble globular, IDR-containing, and IDP classes of proteins in the frozen aqueous solution system.[48] Our results show that EGCG preserves this hallmark feature of the *T*-dependent dynamics of α-syn.

The dynamics and, by extension, the thermal hysteresis of oligomeric $\alpha$-syn in the frozen spin probe mesodomain system have been previously explained with a model put forth by Whitcomb and Warncke.[50] Consideration of the structures of aggregated $\alpha$-syn species is crucial for the application of this model. Specifically, oligomers of different size and conformation have a common NTD/NAC core with the disordered CTD (and some NTD) surrounding and extending outward from this core.[26] In the model, the disordered CTD is principally responsible for the enhanced, cryosolvent-like, solvent dynamics surrounding $\alpha$-syn compared to folded globular proteins, as it disrupts protein and aqueous solvent structure in the neighborhood of the CTD. At high *T*, $W_f$ is dominant for $\alpha$-syn alone, suggesting the majority of TEMPOL is

localized within a fluid mesophase created by the disordered solvent region created by the CTD. Decreasing temperature results in the encroachment of the polycrystalline ice boundary, which exerts confinement on the IDRs surrounding the oligomer core. As this ice boundary closes in, the CTD is packed tightly against other CTDs and the NTD/NAC core domain, excluding TEMPOL and water that had previously inhabited the disordered, fluid, solvent region around the CTD. The excluded water crystalizes along the existing ice boundary, contributing to the growing dominance of the slow mobility component as *T* decreases. At sufficiently low temperatures, the CTD becomes ordered and relatively immobile as a result of ice confinement. As *T* is increased, the tightly packed CTD is less able to disrupt the structure of the surrounding solvent, so the previously excluded water resists melting, which in turn produces more confinement and less mobility at higher temperatures. Thus, thermal hysteresis is observed for aggregated species of $\alpha$-syn.

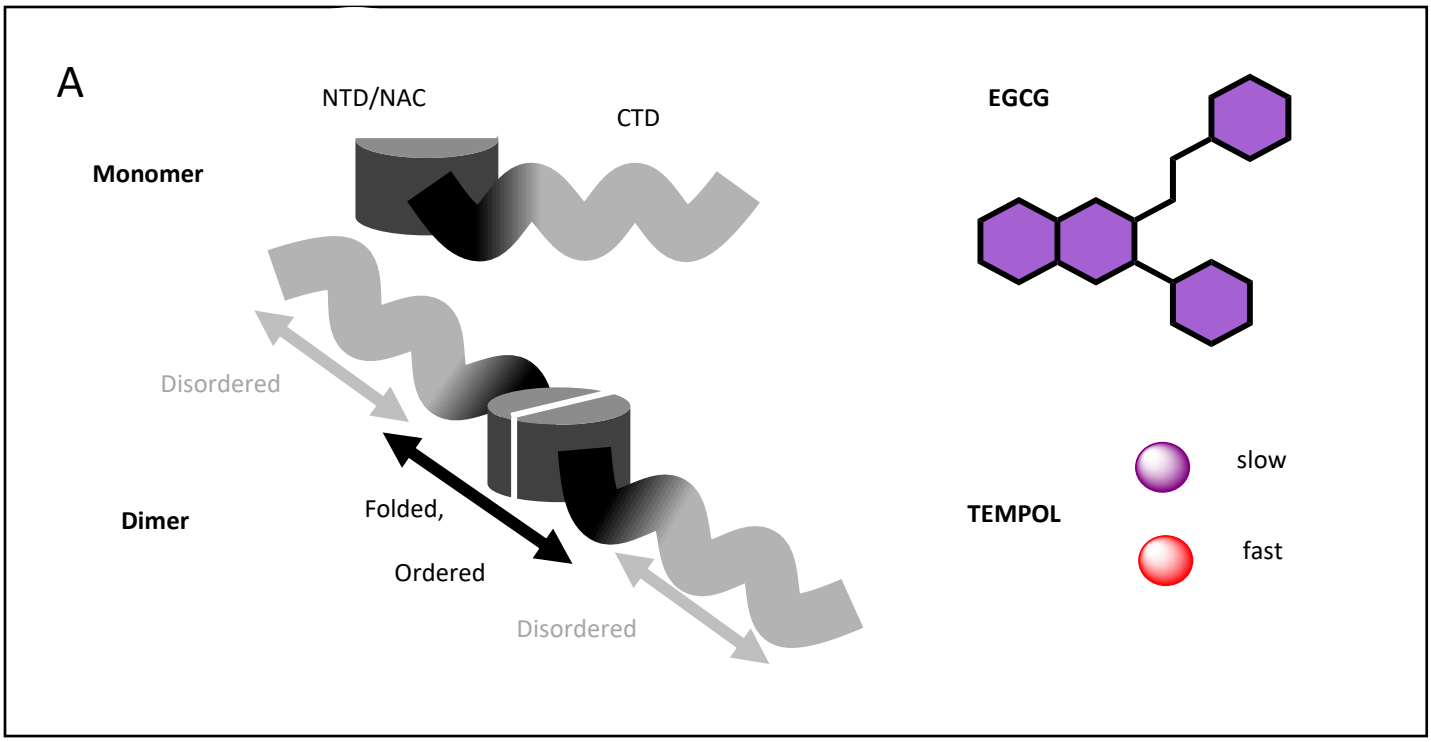
A
NTD/NAC
CTD
Monomer
Disordered
Dimer
Folded,
Ordered
Disordered
EGCG
TEMPOL
slow
fast

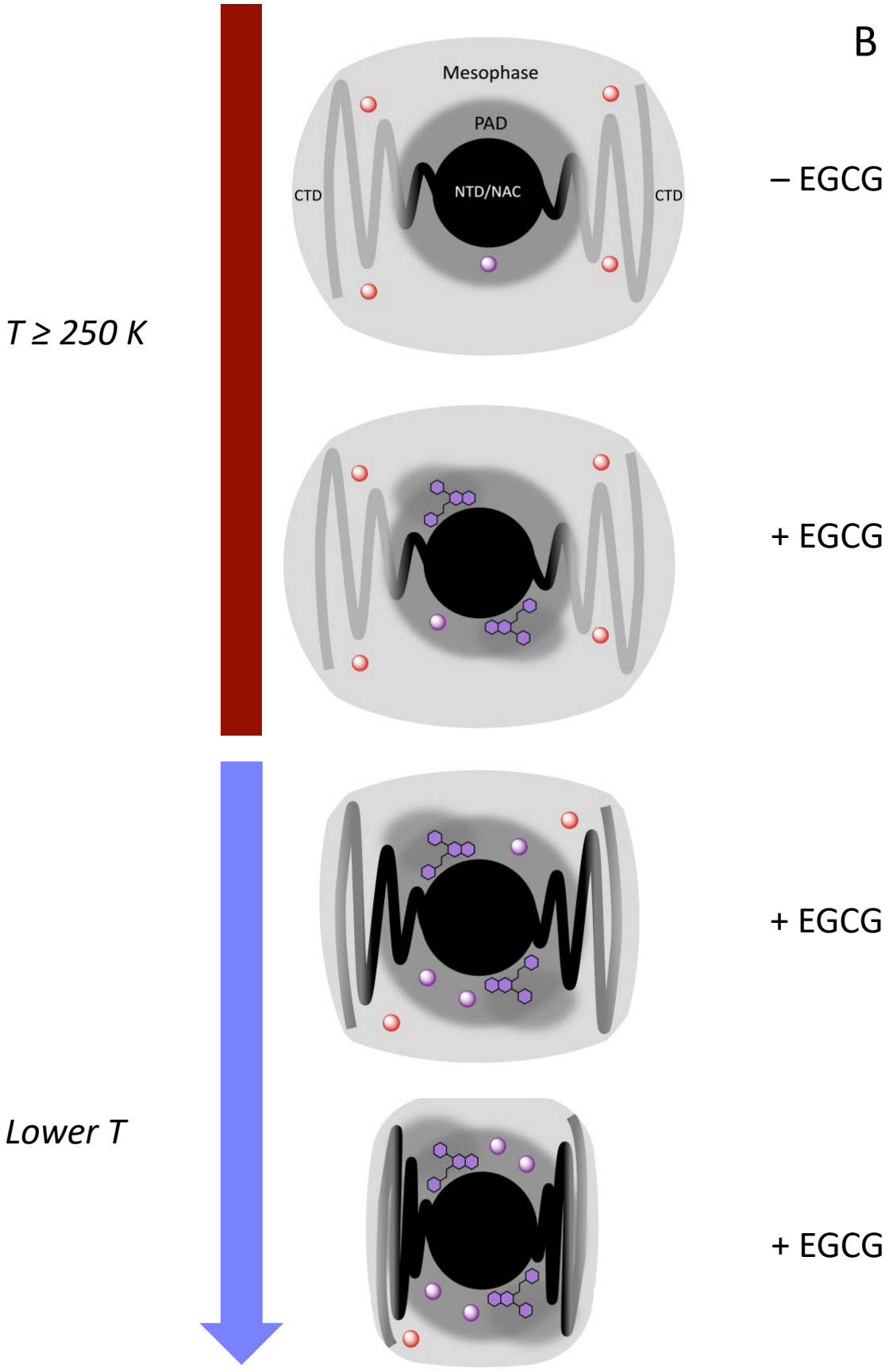
B
Mesophase
PAD
NTD/NAC
CTD
CTD
– EGCG
T ≥ 250 K
+ EGCG
+ EGCG
Lower T
+ EGCG

*Figure 18.* Model for EGCG enhancement of confinement susceptibility in oligomeric $\alpha$-syn. (A) Schematic representations of EPR system components including TEMPOL in slow and fast rotational mobility conditions, EGCG, and $\alpha$-syn monomers and dimers. Mobility of the IDR regions is depicted in grey-scale; low to high mobility corresponds to dark to light. (B) Schematic representation of *T*-dependent confinement of oligomeric $\alpha$-syn in the presence of 1:1 EGCG. Dimers are depicted from above, as in a cross-section of a fibril-like oligomer. Water ice surrounds and confines each dimer structure, transverse (approximately, in plane of the page) to the oligomer NTD/NAC axis (perpendicular to page). In the absence of EGCG, at $T \geq 250$ K, the IDRs of the oligomer create a fluid mesophase; addition of EGCG and subsequent association with the NTD/NAC core of the oligomer contributes to the confinement (compression) of this IDR-mesophase and increases the relative volume of the PAD-like slow mobility phase; decreasing temperature leads to greater confinement by the ice boundary, further packing together the IDRs and diminishing the mesophase volume. Overall, EGCG increases the confinement experienced by oligomeric $\alpha$-syn at all temperatures without significant effect on the dynamics of the IDR-mesophase.

## 7. Summary and Conclusions

This study aimed to characterize the dynamics of oligomeric $\alpha$-syn in the presence of EGCG by utilizing spin probe EPR. The rigid-limit spectra of TEMPOL show that EGCG alone in frozen solution remains solid and immobile throughout the temperature range 200 K $\leq T \leq$ 265 K. However, the frozen solution samples show TEMPOL mobility, and therefore a fluid phase,

upon inclusion of $\alpha$-syn. Consistent with mass spectroscopy,[18] and confocal fluorescence microscopy measurements,[32] our findings indicate that EGCG exerts a concentration dependent effect, further attenuating the mobility of $\alpha$-syn in solution at increasingly higher concentrations. These effects were observed even at equimolar EGCG and $\alpha$-syn (1:1) conditions. Notably, the reduction in $\alpha$-syn dynamics is reflected only in the rotational mobility of the slow, PAD-like, motional component. EPR spectra of frozen solutions of $\alpha$-syn and EGCG reveal that the interactions of $\alpha$-syn with EGCG produce a reactive species capable of eradicating TEMPOL radical signal at elevated temperature, elevated [EGCG], conditions, though these effects were not pronounced at near equimolar conditions or for EGCG alone. EPR spectra of TEMPOL in aqueous $\alpha$-syn+EGCG solution samples display a thermal hysteresis between spectra acquired for increasing *T* and spectra obtained for decreasing *T*.

The interactions of EGCG and $\alpha$-syn can be understood in the context of the model for confinement-resistant dynamics of $\alpha$-syn proposed by Whitcomb and Warncke.[50] Examining the equimolar EGCG/$\alpha$-syn condition, EGCG has a substantial effect on the temperature dependence of the component weights (Fig. 16, $W_{\mathrm{f}}, W_{\mathrm{s}}$). EGCG addition shifts the temperature at "crossover" of the $W_{\mathrm{s}}, W_{\mathrm{f}}$ curves by approximately +10 K. EGCG at 7:1 and 15:1 ratio causes further, small increments in the crossover temperature. Over this low range of EGCG: $\alpha$-syn, there is trend of increasing, $\tau_{\mathrm{c,s}}$, but no change in $\tau_{\mathrm{c,f}}$. Thus, EGCG appears to affect system dynamics predominantly through modulation of the slow mobility solvent phase volume. That is, EGCG produces an increase in $W_{\mathrm{s}}$, and compensating decrease in $W_{\mathrm{f}}$, at each *T* value, with subtle effect on $\tau_{c,s}$ and no effect on $\tau_{c,f}$. Inclusion of EGCG in the frozen mesodomain system thus makes the $\alpha$-syn oligomers more susceptible to the ice boundary confinement, by binding in the NTD/NAC region, and creating an augmenting, local confinement. These results suggest that

EGCG acts through enhancing confinement, and the overall dynamics of the oligomer. This effect is global, because the increased confinement is coupled to the degree of packing of the CTD. The cumulative effect of this increased confinement is a reduction of $W_f$ for each temperature, and EPR spectra become rigid at higher *T* values with increasing [EGCG]. Thermal hysteresis is observed in $\alpha$-syn oligomers in the presence of EGCG, and this is explained by the interaction of EGCG in the NTD/NAC domain. These effects of EGCG on $\alpha$-syn in the 1:1 to 15:1 stoichiometry range suggest that confinement of oligomers in appressed membrane regions *in vivo* reduces the protein dynamics, that are the basis for the destructive dysfunction of membrane disruption and penetration. The TEM and EPR spin probe results indicate that the higher EGCG/$\alpha$-syn ratios of 60:1 and 100:1 represent a different regime, where excess EGCG may form the glassy phase (observed in the EGCG-only sample) that surrounds and compactifies oligomers.

The intrinsically disordered protein, $\alpha$-syn, is thought to play a role in neurotransmitter release and its dysfunction is associated with multiple debilitating neurodegenerative disorders. $\alpha$-Syn exists in monomeric and several aggregate forms; oligomers of $\alpha$-syn have been shown to have particularly high cytotoxicity whilst simultaneously retaining highly dynamic IDRs, making further study of their dynamical properties paramount. Our findings implicate EGCG and other polyphenolic small molecules as avenues for synthesizing therapies for synucleinopathies, as stabilization and immobilization of $\alpha$-syn is associated with reduced cytotoxicity and ability to permeabilize membranes.[29,32] Additionally, these findings offer clarity as to how EGCG interacts with $\alpha$-syn in a concentration-dependent fashion and makes the confinement-resistant CTD more prone to confinement. Further, these findings are aligned with the proposed model[50] for characterizing the dynamical properties of oligomeric $\alpha$-syn.

**References**


1. Uversky, V. N. Neuropathology, biochemistry, and biophysics of α-synuclein aggregation. *J. Neurochem.* **103**, 17–37 (2007).
2. Bendor, J., Logan, T. & Edwards, R. H. The Function of α-Synuclein. *Neuron* **79**, 10.1016/j.neuron.2013.09.004 (2013).
3. Lashuel, H. A., Overk, C. R., Oueslati, A. & Masliah, E. The many faces of α-synuclein: from structure and toxicity to therapeutic target. *Nat. Rev. Neurosci.* **14**, 38–48 (2013).
4. Bertoncini, C. W. *et al.* Release of long-range tertiary interactions potentiates aggregation of natively unstructured α-synuclein. *Proc. Natl. Acad. Sci.* **102**, 1430–1435 (2005).
5. Han, H., Weinreb, P. H. & Lansbury, P. T. The core Alzheimer's peptide NAC forms amyloid fibrils which seed and are seeded by β-amyloid: is NAC a common trigger or target in neurodegenerative disease? *Chem. Biol.* **2**, 163–169 (1995).
6. Uéda, K. *et al.* Molecular cloning of cDNA encoding an unrecognized component of amyloid in Alzheimer disease. *Proc. Natl. Acad. Sci.* **90**, 11282–11286 (1993).
7. Jao, C. C., Hegde, B. G., Chen, J., Haworth, I. S. & Langen, R. Structure of membrane-bound α-synuclein from site-directed spin labeling and computational refinement. *Proc. Natl. Acad. Sci.* **105**, 19666–19671 (2008).
8. Bodner, C. R., Dobson, C. M. & Bax, A. Multiple Tight Phospholipid-Binding Modes of α-Synuclein Revealed by Solution NMR Spectroscopy. *J. Mol. Biol.* **390**, 775–790 (2009).
9. Burré, J. *et al.* α-Synuclein Promotes SNARE-Complex Assembly in Vivo and in Vitro. *Science* **329**, 1663–1667 (2010).

10. Wang, L. *et al.* α-Synuclein Multimers Cluster Synaptic Vesicles and Attenuate Recycling. *Curr. Biol.* **24**, 2319–2326 (2014).

11. Sun, J. *et al.* Functional cooperation of α-synuclein and VAMP2 in synaptic vesicle recycling. *Proc. Natl. Acad. Sci.* **116**, 11113–11115 (2019).

12. Eliezer, D., Kutluay, E., Bussell, R. & Browne, G. Conformational properties of α-synuclein in its free and lipid-associated states11Edited by P. E. Wright. *J. Mol. Biol.* **307**, 1061–1073 (2001).

13. Gracia, P., Camino, J. D., Volpicelli-Daley, L. & Cremades, N. Multiplicity of α-Synuclein Aggregated Species and Their Possible Roles in Disease. *Int. J. Mol. Sci.* **21**, 8043 (2020).

14. Sandal, M. *et al.* Conformational Equilibria in Monomeric α-Synuclein at the Single-Molecule Level. *PLOS Biol.* **6**, e6 (2008).

15. Milovanovic, D., Wu, Y., Bian, X. & De Camilli, P. A Liquid Phase of Synapsin and Lipid Vesicles. *Science* **361**, 604–607 (2018).

16. Ray, S. *et al.* α-Synuclein aggregation nucleates through liquid–liquid phase separation. *Nat. Chem.* **12**, 705–716 (2020).

17. Neupane, K., Solanki, A., Sosova, I., Belov, M. & Woodside, M. T. Diverse Metastable Structures Formed by Small Oligomers of α-Synuclein Probed by Force Spectroscopy. *PLOS ONE* **9**, e86495 (2014).

18. Grønnemose, A. L., Østerlund, E. C., Otzen, D. E. & Jørgensen, T. J. D. EGCG has dual and opposing effects on the N-terminal region of self-associating α-synuclein oligomers. *J. Mol. Biol.* 167855 (2022) doi:10.1016/j.jmb.2022.167855.

19. Alam, P., Bousset, L., Melki, R. & Otzen, D. E. α-synuclein oligomers and fibrils: a spectrum of species, a spectrum of toxicities. *J. Neurochem.* **150**, 522–534 (2019).

20. Heise, H. *et al.* Molecular-level secondary structure, polymorphism, and dynamics of full-length α-synuclein fibrils studied by solid-state NMR. *Proc. Natl. Acad. Sci.* **102**, 15871–15876 (2005).

21. Tuttle, M. D. *et al.* Solid-state NMR structure of a pathogenic fibril of full-length human α-synuclein. *Nat. Struct. Mol. Biol.* **23**, 409–415 (2016).

22. Li, Y. *et al.* Amyloid fibril structure of α-synuclein determined by cryo-electron microscopy. *Cell Res.* **28**, 897–903 (2018).

23. Guerrero-Ferreira, R., Kovacik, L., Ni, D. & Stahlberg, H. New insights on the structure of alpha-synuclein fibrils using cryo-electron microscopy. *Curr. Opin. Neurobiol.* **61**, 89–95 (2020).

24. Anderson, J. P. *et al.* Phosphorylation of Ser-129 Is the Dominant Pathological Modification of α-Synuclein in Familial and Sporadic Lewy Body Disease*. *J. Biol. Chem.* **281**, 29739–29752 (2006).

25. Spillantini, M. G. *et al.* α-Synuclein in Lewy bodies. *Nature* **388**, 839–840 (1997).

26. Cremades, N., Chen, S. W. & Dobson, C. M. Chapter Three - Structural Characteristics of α-Synuclein Oligomers. in *International Review of Cell and Molecular Biology* (ed. Sandal, M.) vol. 329 79–143 (Academic Press, 2017).

27. Chen, S. W. *et al.* Structural characterization of toxic oligomers that are kinetically trapped during α-synuclein fibril formation. *Proc. Natl. Acad. Sci. U. S. A.* **112**, E1994-2003 (2015).

28. Lorenzen, N. *et al.* The Role of Stable α-Synuclein Oligomers in the Molecular Events Underlying Amyloid Formation. *J. Am. Chem. Soc.* **136**, 3859–3868 (2014).

29. Andersen, C. B., Yoshimura, Y., Nielsen, J., Otzen, D. E. & Mulder, F. A. A. How epigallocatechin gallate binds and assembles oligomeric forms of human alpha-synuclein. *J. Biol. Chem.* **296**, 100788 (2021).

30. Takahashi, R. *et al.* Phenolic compounds prevent the oligomerization of α-synuclein and reduce synaptic toxicity. *J. Neurochem.* **134**, 943–955 (2015).

31. Caruana, M. *et al.* Inhibition and disaggregation of α-synuclein oligomers by natural polyphenolic compounds. *FEBS Lett.* **585**, 1113–1120 (2011).

32. Lorenzen, N. *et al.* How Epigallocatechin Gallate Can Inhibit α-Synuclein Oligomer Toxicity in Vitro♦. *J. Biol. Chem.* **289**, 21299–21310 (2014).

33. Fusco, G. *et al.* Structural basis of membrane disruption and cellular toxicity by α-synuclein oligomers. *Science* **358**, 1440–1443 (2017).

34. Weinreb, O., Amit, T., Mandel, S. & Youdim, M. B. H. Neuroprotective molecular mechanisms of (−)-epigallocatechin-3-gallate: a reflective outcome of its antioxidant, iron chelating and neuritogenic properties. *Genes Nutr.* **4**, 283–296 (2009).

35. Bieschke, J. *et al.* EGCG remodels mature α-synuclein and amyloid-β fibrils and reduces cellular toxicity. *Proc. Natl. Acad. Sci.* **107**, 7710–7715 (2010).

36. Ehrnhoefer, D. E. *et al.* EGCG redirects amyloidogenic polypeptides into unstructured, off-pathway oligomers. *Nat. Struct. Mol. Biol.* **15**, 558–566 (2008).

37. Dong, J., Hubel, A., Bischof, J. C. & Aksan, A. Freezing-Induced Phase Separation and Spatial Microheterogeneity in Protein Solutions. *J. Phys. Chem. B* **113**, 10081–10087 (2009).

38. Qin, Y., Wang, L. & Zhong, D. Dynamics and mechanism of ultrafast water–protein interactions. *Proc. Natl. Acad. Sci. U. S. A.* **113**, 8424–8429 (2016).

39. Lewandowski, J. R., Halse, M. E., Blackledge, M. & Emsley, L. Direct observation of hierarchical protein dynamics. *Science* **348**, 578–581 (2015).

40. Li, W., Nforneh, B., Whitcomb, K. L. & Warncke, K. Resolution and characterization of confinement- and temperature-dependent dynamics in solvent phases that surround proteins in frozen aqueous solution by using spin-probe EPR spectroscopy. *Methods Enzymol.* **666**, 25–57 (2022).

41. Stoll, S. & Schweiger, A. EasySpin, a comprehensive software package for spectral simulation and analysis in EPR. *J. Magn. Reson.* **178**, 42–55 (2006).

42. Nforneh, B. & Warncke, K. Mesodomain and Protein-Associated Solvent Phases with Temperature-Tunable (200–265 K) Dynamics Surround Ethanolamine Ammonia-Lyase in Globally Polycrystalline Aqueous Solution Containing Dimethyl Sulfoxide. *J. Phys. Chem. B* **121**, 11109–11118 (2017).

43. Nforneh, B. & Warncke, K. Control of Solvent Dynamics around the B12-Dependent Ethanolamine Ammonia-Lyase Enzyme in Frozen Aqueous Solution by Using Dimethyl Sulfoxide Modulation of Mesodomain Volume. *J. Phys. Chem. B* **123**, 5395–5404 (2019).

44. Frauenfelder, H. *et al.* A unified model of protein dynamics. *Proc. Natl. Acad. Sci.* **106**, 5129–5134 (2009).

45. Sato, H. *et al.* Electron spin-lattice relaxation of nitroxyl radicals in temperature ranges that span glassy solutions to low-viscosity liquids. *J. Magn. Reson. San Diego Calif 1997* **191**, 66–77 (2008).

46. Ionescu, A., Li, W., Nforneh, B. & Warncke, K. Coupling of ethanolamine ammonia-lyase protein and solvent dynamics characterized by the temperature-dependence of EPR spin probe mobility and dielectric permittivity. *J. Chem. Phys.* **154**, 175101 (2021).

47. Arakawa, T., Kita, Y. & Timasheff, S. N. Protein precipitation and denaturation by dimethyl sulfoxide. *Biophys. Chem.* **131**, 62–70 (2007).

48. Li, W., Whitcomb, K. L. & Warncke, K. Confinement dependence of protein-associated solvent dynamics around different classes of proteins, from the EPR spin probe perspective. *Phys. Chem. Chem. Phys.* **24**, 23919–23928 (2022).

49. Bhat, S. N., Sharma, A. & Bhat, S. V. Vitrification and Glass Transition of Water: Insights from Spin Probe ESR. *Phys. Rev. Lett.* **95**, 235702 (2005).

50. Whitcomb, K. L. & Warncke, K. Confinement-Resistant Dynamics of Oligomeric and Fibrillar Alpha-Synuclein. *submitted* (2023).

51. Wang, M., Zhu, C., Kohne, M. M. & Warncke, K. Resolution and characterization of chemical steps in enzyme catalytic sequences by using low temperature and time-resolved, full-spectrum EPR spectroscopy in fluid cryosolvent and frozen solution systems. *Methods Enzymol.* **563**, 59–94 (2015).

52. Cao, Y., Teng, J. & Selbo, J. Amorphous Solid Dispersion of Epigallocatechin Gallate for Enhanced Physical Stability and Controlled Release. *Pharmaceuticals* **10**, 88 (2017).

53. Lorenzen, N., Lemminger, L., Pedersen, J. N., Nielsen, S. B. & Otzen, D. E. The N-terminus of α-synuclein is essential for both monomeric and oligomeric interactions with membranes. *FEBS Lett.* **588**, 497–502 (2014).

54. Ahmed, R. *et al.* Molecular Mechanism for the (−)-Epigallocatechin Gallate-Induced Toxic to Nontoxic Remodeling of Aβ Oligomers. *J. Am. Chem. Soc.* **139**, 13720–13734 (2017).